Institute of Architecture of Application Systems

University of Stuttgart
Universitätsstraße 38
D–70569 Stuttgart

Masterarbeit

Investigating Gate Teleportation Using Non-Maximally Entangled States for Gate Cutting

Moritz Hildebrand

Course of Study:	Informatik
Examiner:	Prof. Dr. Dr. h. c. Frank Leymann
Supervisor:	Marvin Bechtold, M.Sc.
Commenced:	December 5, 2023
Completed:	June 5, 2024

Abstract

Quantum computing can solve complex problems that are beyond the reach of classical computers. Despite its vast potential, the field of quantum computing is currently hindered by significant challenges, particularly when it comes to scaling up the size of quantum devices. One of the major limitations of current quantum computers is the restricted number of qubits they can effectively utilize. Distributed quantum computing offers a promising solution to this problem by aggregating the computational power of multiple deficient quantum computers. Two techniques for distributed quantum computing that have shown great promise in this domain are gate teleportation and gate cutting. However, both techniques have drawbacks. Gate teleportation requires shared entanglement and gate cutting incurs a sampling overhead. This thesis aims to explore how these techniques can be combined potentially mitigating their drawbacks. In this thesis, we investigate the error that non-maximally entangled (NME) resource states cause in the gate teleportation of controlled gates. We present different mathematical decompositions of the error, which facilitate gate cuts. Using these gate cuts we demonstrate that NME states can reduce the sampling overhead of the cuts. The result is a trade-off between the degree of entanglement of the resource states and the sampling overhead of the cuts.

Kurzfassung

Quantencomputer haben das Potenzial, komplexe Probleme zu lösen, die die Möglichkeiten eines klassischen Computers übersteigen. Trotz des immensen Potenzials der Quanteninformatik gibt es praktische Hürden, die die Realisierung eines fehlertoleranten Quantencomputers behindern. Eine wesentliche Hürde ist die begrenzte Anzahl an Qubits heutiger Quantencomputer. Das Konzept des verteilten Quantum-Computings bietet einen vielversprechenden Lösungsansatz, bei dem die Rechenleistung mehrerer kleiner Quantencomputer vereint wird. Die Gate-Teleportation und das Gate-Cutting sind zwei aufstrebende Techniken im Bereich des verteilten Quanten-Computings, beide mit gewissen Nachteilen. Die Gate-Teleportation benötigt einen maximal verschränkten Zustand, der auf die entsprechenden Quantencomputer verteilt ist, während das Gate-Cutting zusätzliche Ausführungen von Teilschaltkreisen erfordert. Diese Thesis hat das Ziel, die Gate-Teleportation und das Gate-Cutting mittels nicht maximal verschränkter (NME) Zustände zu vereinen. In dieser Thesis untersuchen wir den Fehler, den NME-Ressourcenzustände bei der Gate-Teleportation von kontrollierten Gattern verursachen. Wir präsentieren verschiedene mathematische Zerlegungen des Fehlers, die Gate-Cuts ermöglichen. Anhand der von uns entdeckten Gate-Cuts demonstrieren wir, dass NME-Zustände genutzt werden können, um den Sampling-Overhead der Cuts zu verringern. Das Ergebnis ist ein Trade-off zwischen dem Verschränkungsgrad der Ressourcenzustände und dem Sampling-Overhead der Cuts.

Contents

List of Figures

Acronyms

CNOT controlled NOT. 15

CZ controlled-Z. 18

LOCC local operations and classical communication. 15

MCZ multi-controlled Z. 41

MPC measurement-and-prepare channels. 40

NME non-maximally entangled. 11

1 Introduction

Quantum computing has emerged as a revolutionary technology with the potential to solve complex problems beyond the capabilities of classical computers [AAB+19; Gro96; HM17; Sho]. Despite its promise, the field faces significant challenges, particularly in scaling up quantum devices [CTV17; GPAY23; MK13; Pre18]. Current quantum computers are limited by the number of qubits they can effectively utilize and by the errors that accumulate during computations [GCS17; KBF+15]. These constraints hinder the execution of large-scale quantum algorithms, which are essential to realizing the full potential of quantum computing.

Distributed quantum computing offers a promising solution to these limitations by interconnecting multiple smaller quantum devices into a unified system [CCB18; Cuo23; FYKI12]. This approach leverages the ability to exchange both classical and quantum information between devices, enabling them to collaboratively perform larger computations than would be possible individually [CAF+22]. The concept of distributed quantum computing is akin to distributed classical computing, where tasks are divided among multiple processors to enhance computational power and efficiency.

To facilitate distributed quantum computing, two promising techniques have emerged: circuit cutting and quantum teleportation [BBC+93; PHOW20]. Circuit cutting involves dividing a large quantum circuit into subcircuits that can be executed on smaller quantum devices. This can be done in two ways: by wire cutting, where individual qubits are cut, or by gate cutting, where specific quantum gates are split across different devices. Although circuit cutting enables larger computations by leveraging multiple quantum processors, it introduces an exponential sampling overhead, requiring repeated measurements to reconstruct the original computation from its parts [PS23].

Quantum teleportation, on the other hand, leverages entanglement to transfer quantum information between different devices [BBC+93]. This technique requires the use of maximally entangled states to enable the transmission of a quantum state through classical communication channels. While quantum teleportation works without additional sampling overhead the generation and maintenance of maximally entangled states pose significant practical challenges [AAS23; KMSD19]. Ensuring high-fidelity entanglement over long distances remains a major hurdle, limiting the scalability of this approach.

Recent work by Bechtold et al. [BBLM23; BBLM24] presents an innovative approach to mitigate these drawbacks by using non-maximally entangled (NME) states as resource states for quantum teleportation. Their technique creates a continuum between quantum teleportation and circuit cutting, where the degree of entanglement in the resource state dictates the required sampling overhead. Specifically, using NME states with lower entanglement increases the sampling overhead, while higher entanglement reduces it, offering a flexible trade-off between computational cost and entanglement resources.

However, there is a gap in research regarding the application of NME states to reduce the sampling overhead in gate cutting. This thesis aims to bridge this gap by investigating how gate teleportation with NME states can be used for gate cutting. Gate teleportation describes variants of the quantum teleportation protocol that allow the implementation of quantum gates across different devices using entangled resource states and classical communication [EJPP00]. The primary goal of this thesis is to explore known gate teleportation approaches, identifying gates that can be teleported and examining how NME resource states influence the teleportation process. A particular focus is placed on identifying and correcting errors that arise when NME states are employed, aiming to optimize the feasibility and efficiency of distributed quantum computation in the face of current technological limitations.

The remainder of this thesis is organized as follows. Chapter 2 lays the knowledge foundation by introducing the preliminaries necessary for understanding gate teleportation with NME states and gate cutting. It also covers required quantum computing concepts. The subsequent Chapter 3 presents our findings on gate teleportation with NME states and explores how it can be applied to gate cutting. Chapter 4 details numerical experiments that validate our theoretical results. In Chapter 5 we discuss our findings and in Chapter 6, we contextualize our research within the broader field of distributed quantum computing. Finally, we conclude with a summary of our work in Chapter 7. Additional calculations supporting our findings are provided in Appendix A.

2 Background

Investigating gate teleportation with NME states involves adjusting key parameters in the gate teleportation process. Entanglement is the core quantum mechanical resource that lies at the heart of quantum teleportation. Therefore, we first define the notion of NME states. Equipped with the concept of NME states, we turn our attention to the theory of quantum teleportation. We describe the quantum teleportation protocol as a prerequisite for gate teleportation. Both protocols enable quantum information transfer between two parties using entanglement and classical communication. Gate teleportation is a variant of the quantum teleportation protocol that applies a quantum operation to the transferred quantum information during the teleportation process. Next, in preparation for harnessing gate teleportation with NME states in distributed computing, we present the introductory principles of circuit cutting. We close this section by introducing two quantum computing concepts: the deferred measurement principle and the Hadamard test.

2.1 Quantum Entanglement

Quantum entanglement is a key concept in quantum mechanics that reveals a deep connection between quantum particles, even if they are spatially separated. When particles interact, they can become entangled, creating a shared state where they can no longer be described individually — they act as one interconnected system. Mathematically, entanglement is defined as the inability to express the state of a joint quantum system as a tensor product of the states of its components. Specifically, in a system composed of two qubits in distinct Hilbert spaces H_A and H_B, the joint state $|\psi\rangle$ is deemed entangled if it cannot be represented as a product state, i.e., $|\psi\rangle \neq |\psi_A\rangle \otimes |\psi_B\rangle$ [22]. One of the most remarkable properties of entangled states is that when one qubit is measured, the measurement outcome instantaneously provides information about the state of the other qubit. When two qubits are maximally entangled, this means that the information about the state of one qubit provides complete information about the state of the other qubit. There exist four Bell states, denoted $|\Phi^+\rangle$, $|\Phi^-\rangle$, $|\Psi^+\rangle$ and $|\Psi^-\rangle$, each exemplifying maximal entanglement between two qubits. They can be seen in the Equations (2.1) to (2.4).

$$|\Phi^+\rangle = \frac{1}{\sqrt{2}} |00\rangle + |11\rangle \tag{2.1}$$

$$|\Phi^-\rangle = \frac{1}{\sqrt{2}} |00\rangle - |11\rangle \tag{2.2}$$

$$|\Psi^+\rangle = \frac{1}{\sqrt{2}} |01\rangle + |10\rangle \tag{2.3}$$

$$|\Psi^-\rangle = \frac{1}{\sqrt{2}} |01\rangle - |10\rangle \tag{2.4}$$

Entanglement manifests in various degrees, ranging from maximal entanglement to partial entanglement or no entanglement at all. But before addressing different degrees of entanglement, we introduce a powerful tool to represent composite systems: the Schmidt decomposition. The Schmidt decomposition offers a precise means of representing any pure bipartite state, denoted as $|\psi\rangle$, in a structured format. According to the Schmidt decomposition theorem, any such pure state $|\psi\rangle$ belonging to a composite system $H_A \otimes H_B$ can be expressed as [22]:

$$|\psi\rangle = \sum_{i \in \{0,1\}} c_i \, |i_A\rangle \, |i_B\rangle \tag{2.5}$$

Here, $|i_A\rangle$ and $|i_B\rangle$ represent orthonormal bases for the respective Hilbert spaces of the subsystems H_A and H_B, while $c_i \in \mathbb{R}_{\geq 0}$ symbolize the Schmidt coefficients, ensuring that $\sum_i c_i = 1$. The Schmidt rank, denoted as the number of non-zero Schmidt coefficients, quantifies the degree of entanglement between the subsystems. Utilizing the Schmidt decomposition, any two-qubit quantum state $|\psi\rangle$ can be represented as:

$$|\psi\rangle = c_0 \, |0_A\rangle \, |0_B\rangle + c_1 \, |1_A\rangle \, |1_B\rangle \tag{2.6}$$

$$= c_0 \left(|0_A 0_B\rangle + \frac{c_1}{c_0} \, |1_A 1_B\rangle \right) \tag{2.7}$$

This formulation extends to encompass all two-qubit NME states. As teleportation protocols typically employ the first Bell state $|\Phi^+\rangle$ when necessitating a maximally entangled state, we utilize its extension $|\Phi^k\rangle$ in our work. $|\Phi^k\rangle$ is defined in Equation (2.8) where $k \in \mathbb{R}_{\geq 0}$.

$$|\Phi^k\rangle := \frac{1}{\sqrt{1+k^2}} (|00\rangle + k \, |11\rangle) \tag{2.8}$$

Analogous generalizations can be made for the other Bell states. $|\Phi^k\rangle$ exhibits varying degrees of entanglement. Remarkably, $|\Phi^k\rangle$ is separable for $k = 0, k \to \infty$:

$$|\Phi^0\rangle = |00\rangle \tag{2.9}$$

$$|\Phi^{k\to\infty}\rangle = |11\rangle \tag{2.10}$$

and as $k \to 1$ the degree of entanglement increases until it is maximal for $k = 1$:

$$|\Phi^1\rangle = |\Phi^+\rangle \tag{2.11}$$

The combination of the generalized state $|\Phi^k\rangle$ with single-qubit operations is sufficient to represent every possible two-qubit state, whether entangled or not. Any such state $|\psi\rangle$ can be re-expressed as $|\psi\rangle = (A \otimes B) \, |\Phi^k\rangle$, where A and B are local unitary transformations.

Entangling two physically connected qubits can be achieved through a quantum circuit. For the creation of Bell states refer to Nielsen and Chuang [NC12]. However, in practice, current noisy quantum hardware presents several challenges in forming entangled states [GTC22; WJEK99]. These challenges include the need for precise synchronization and effective error correction and mitigation techniques [CCC20; CCT+20; CCVH20]. For many quantum information protocols, such as quantum teleportation, entanglement must be established in advance between two remote parties. In practice, the inevitable interaction of entangled subsystems with the environment during distribution and storage leads to the degradation of entanglement [AAS23]. Consequently, leveraging the usage of NME states can be beneficial [DWLJ23; PP19; PV12; WTYK15]. Furthermore, there lies theoretical value in the utilization of NME states. For instance, using NME states in quantum teleportation has been shown to balance the degree of entanglement with the additional sampling overhead required in circuit cutting techniques [BBLM23].

2.2 Quantum Teleportation

Quantum teleportation is a process in which the exact state of a quantum system is transmitted from one location to another without physically transporting the particle. When Alice and Bob want to teleport a quantum state $|\psi\rangle$, they initially share a maximally entangled pair of qubits. Although any of the four Bell pairs can be utilized for quantum teleportation, we opt to demonstrate the quantum teleportation protocol in its most common form, employing the first Bell state $|\Phi^+\rangle$ as resource state [BBC+93]. The quantum teleportation circuit is depicted in Figure 2.1.

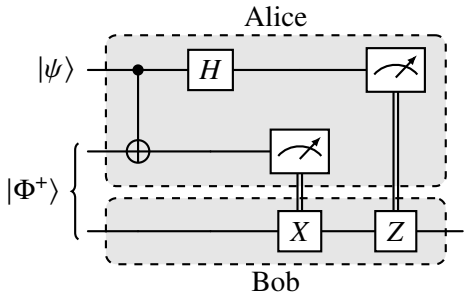

Figure 2.1: Quantum teleportation circuit.

In the given scenario, Alice has two qubits: one carrying the quantum state $|\psi\rangle$ and her share of the entangled Bell pair. Meanwhile, Bob possesses one qubit, representing his portion of the entangled Bell pair. Alice and Bob employ local operations and classical communication (LOCC) to transmit the quantum state $|\psi\rangle$ from Alice's qubit to Bob's qubit. Alice performs a sequence of operations to initiate the quantum teleportation process. First, she applies the controlled NOT (CNOT) gate, with $|\psi\rangle$ serving as the control qubit to her qubits, followed by a Hadamard gate on the qubit initially holding $|\psi\rangle$. Subsequently, Alice measures her two qubits and transmits the measurement outcomes to Bob via classical communication. This procedure inevitably leads to the destruction of the shared entangled state between Alice and Bob. Bob's role in the process is to reconstruct the state $|\psi\rangle$ from his share of the entangled state. Depending on the measurement results received from Alice, Bob performs corrective operations. Specifically, if the qubit holding Alice's portion of the entangled pair measures $|1\rangle$, Bob applies a Pauli-X gate to his qubit. Additionally, if the measurement of Alice's qubit, which originally held $|\psi\rangle$, returns $|1\rangle$, Bob applies a Z gate. However, if any measurement yields $|0\rangle$, Bob refrains from applying the corresponding gate.

If a NME state is used as the shared resource in the quantum teleportation protocol, the teleportation cannot be achieved with unit fidelity and unit probability simultaneously [AP02]. However, it is still possible to teleport an unknown quantum state probabilistically with unit fidelity or with reduced fidelity but higher probability [YY10].

2.3 Gate Teleportation

Gate teleportation is a concept in quantum information theory that builds on quantum teleportation, allowing non-local quantum gates to be applied through LOCC. Unlike quantum teleportation, gate teleportation includes a variety of different circuits that implement different quantum gates. Our focus is on gate teleportation circuits that support distributed quantum computing, where Alice has

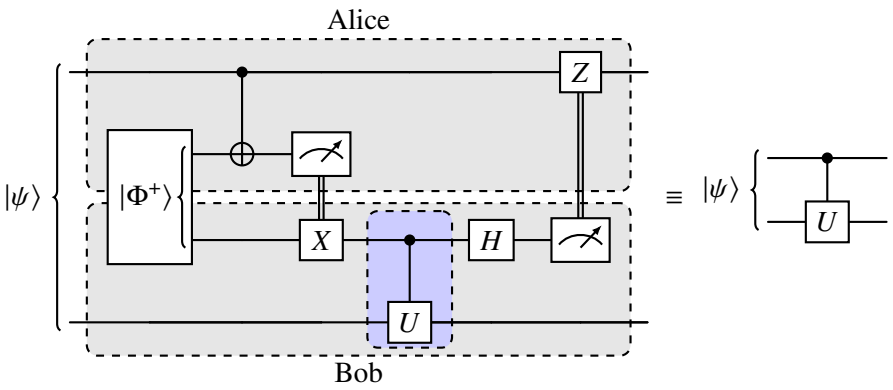

Figure 2.2: Gate teleportation circuit for controlled gates [EJPP00].

a qubit, Bob has a qubit, and they wish to apply a two-qubit gate to their qubits while both end up with their respective result state. This concept is illustrated through the gate teleportation circuit that forms the basis for our research. The circuit shown in Figure 2.2 originally introduced by Eisert et al. [EJPP00], applies an arbitrarily controlled two-qubit quantum gate to two physically separated qubits, one belonging to Alice and the other to Bob. Throughout this thesis, we assume a two-qubit controlled gate CU has the form shown in Equation (2.12), where $\oplus$ denotes the direct sum and U is an arbitrary single-qubit gate matrix.

$$CU := I \oplus U = \begin{bmatrix} I & 0 \\ 0 & U \end{bmatrix} \tag{2.12}$$

In Figure 2.2, Alice and Bob initially share a Bell pair, and both qubits of the Bell pair undergo local operations and measurements. The measurement results are then communicated via classical communication channels, with a total of two classical bits transmitted.

Next, we compare the controlled gate teleportation circuit shown in Figure 2.2 with the naive distributed computing approach that arises from the quantum teleportation protocol directly. We depict the circuit for this approach in Figure 2.3. In this naive approach, Alice teleports her qubit to Bob, who then applies the two-qubit operation. Afterward, Bob teleports Alice's modified state back. While this naive approach is functional, it is less resource-efficient because it requires two instances of the quantum teleportation protocol. This means the requirement of two shared Bell pairs and four classical bits for communication, in contrast to the single Bell pair and two classical bits of communication required by the controlled gate teleportation circuit. This naturally raises the question of whether a more resource-efficient circuit than the naive approach can be devised for general two-qubit gates. But this is not the case. Research by Stahlke and Griffiths [SG11] explores the minimal entanglement resources required for the deterministic execution of a non-local two-qubit unitary operation. The study establishes that the operator's Schmidt rank is a limiting factor in determining these bounds. Specifically, the Schmidt rank of the resource state must be at least as high as the Schmidt rank of the unitary operation to be teleported. For a non-zero two-qubit operator $X \in \mathbb{C}^{4\times4}$, the operator's Schmidt rank is defined as the number of terms in the decomposition

$$X = \sum_i A_i \otimes B_i, \tag{2.13}$$

where $\{A_i\}$ and $\{B_i\}$ are orthogonal subsets of non-zero operators in $\mathbb{C}^{2\times2}$ [MN18].

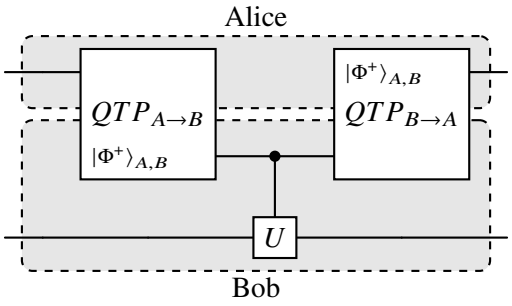

Figure 2.3: Naive distributed quantum computing approach based on quantum teleportation. $|\Phi^+\rangle_{A,B}$ denotes a Bell pair in the state $|\Phi^+\rangle$ shared between Alice and Bob. The $QTP_{X\to Y}$ gate denotes the quantum teleportation protocol that teleports a quantum state from one party X to another party Y.

According to Müller-Hermes and Nechita [MN18], two-qubit gates can have Schmidt ranks of 1, 2, or 4. A Schmidt rank of 1 indicates a product (separable) unitary, which does not create entanglement between qubits. Unitaries with a Schmidt rank of 2 are effectively controlled unitaries with some degree of non-local entanglement. All unitaries of Schmidt rank 2 can be decomposed in one controlled gate and single-qubit operations [CY13]. Unitaries with Schmidt rank 4 represent more complex non-local bipartite entangling operations that go beyond controlled gates.

Recall that a Bell pair has a Schmidt rank of 2. Consequently, the circuit shown in Figure 2.2 is optimal for controlled quantum gates in terms of entanglement resources. Furthermore, not all two-qubit gates can be teleported using only one Bell pair as a resource state. Specifically, operators with a Schmidt rank of 4 require two Bell pairs for teleportation. This makes the naive approach from Figure 2.3 a reasonable choice for operators with Schmidt rank 4, which is why we concentrate in this thesis on teleporting controlled gates.

2.4 Circuit Cutting

Circuit cutting is a technique used in quantum computing to decompose a large quantum circuit into smaller subcircuits, allowing the execution on limited quantum hardware [TTS+21]. The main purpose of circuit cutting is to enable the execution of large quantum circuits that exceed the qubit capacity or depth constraints of current quantum computers. By cutting the circuit into smaller parts, the resource requirements are reduced to fit within the limitations of the available hardware [CHL+23]. This approach can also help to reduce the impact of hardware noise and errors [PSSO21].

When cutting a circuit, each subcircuit can be executed independently, and their outcomes are combined to reconstruct the original circuit's result. Circuit cutting typically involves two types of cuts: wire cuts and gate cuts. Wire cuts involve severing specific qubit connections within a quantum circuit and partitioning it into subcircuits by interrupting the flow of quantum information along those connections. In contrast, gate cuts replace specific gates in the circuit, dividing it at those gate locations. Gate cuts might require inserting additional gates to enable the partitioning process.

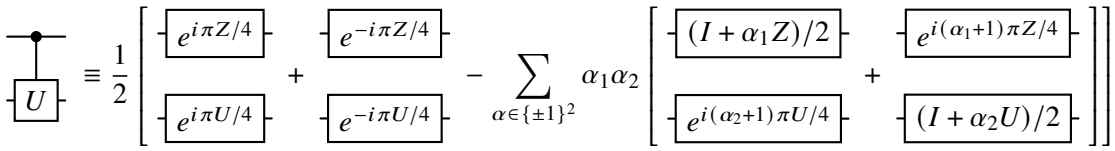

Figure 2.4: Single-qubit decomposition of the controlled-{X,Y,Z,H} gate ($U \in \{X, Y, Z, H\}$) [MF21].

Subcircuits in a gate decomposition are not necessarily weighted the same. Each subcircuit has an associated weighting factor, which is directly linked to its required number of executions. Every time a quantum circuit is cut, there's a sampling overhead incurred due to the measurement operations needed to divide the circuit. This overhead represents the factor by which the number of shots of the original circuit must be multiplied to maintain the same error accuracy for the decomposed circuits. For instance, if a circuit is decomposed into two decomposition circuits with each being weighted by $\frac{1}{2}$, the overhead is 1, implying no additional shots are needed. However, if each decomposed circuit has a weighting factor of 1, the overhead becomes 2, necessitating twice as many shots overall. With each additional cut, the circuits are further decomposed, multiplying the number of shots by all the overheads, leading to an exponential increase in the shots required to maintain the same error accuracy. The cost of wire cutting without classical communication between subcircuits scales as $O(16^n)$ but reduces to $O(4^n)$ with classical communication, where n represents the number of cut wires [BPS23]. The cost of gate cuts depends on various factors, including the number and location of the cuts, the structure of the circuit, and specific cutting and reconstruction techniques, also exhibiting exponential growth [BPK24; MF21; SPS23; UPR+23].

The decomposition of the controlled-Z (CZ) gate by Mitarai and Fujii [MF21] provides a relevant example of gate cutting for this thesis. In Figure 2.4, we present a slightly more general variation of the CZ gate decomposition that also covers the controlled-X, -Y, and -H gates. We verify this decomposition in Appendix A.1. Rather than executing these controlled gates directly, we can divide the circuit into 10 separate circuits, execute them independently, and then combine the results. Notice that each of these 10 circuits replaces the controlled gate with two single-qubit operations, creating a gate cut. It is important to recognize that instead of running just one circuit, we now need to execute 10 separate circuits. However, each of these circuits in the decomposition is weighted by $\frac{1}{2}$, indicating that we need to execute each of them only half the number of shots as the original circuit to maintain the same error rate. This results in a sampling overhead of $\frac{10}{2} = 5$.

Both gate teleportation and circuit cutting enable distributed quantum computing, but they have their drawbacks. Gate teleportation relies on entanglement resources to deterministically decompose a non-local gate, while circuit cutting's exponential sampling overhead results from additional measurement and reconstruction steps. This encourages us to explore possible connections among these limitations to find ways to reduce the sampling overhead by leveraging entanglement resources. Bechtold et al. [BBLM23] have already shown a connection between wire cutting and quantum teleportation, providing a technique that trades off the degree of entanglement with sampling overhead.

2.5 Deferred Measurement Principle

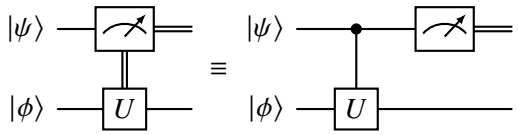

Figure 2.5: Deferred measurement principle applied to a measurement-controlled U gate.

In quantum teleportation, Alice and Bob solely exchange classical information. The measurement outcomes, conveyed through classical communication channels, subsequently dictate corrective operations at the receiving end. Given the frequent occurrence of such measurement-controlled operations in our investigations, it is advantageous to express them conveniently within quantum computations. The deferred measurement principle offers a helpful approach in this regard. It states that any quantum circuit with intermediate measurements can be transformed into an equivalent circuit in which all measurements are deferred until the end of the computation, without affecting the final outcome [NC12]. Figure 2.5 shows how a measurement-controlled quantum gate is converted into a controlled gate followed by measuring the control qubit using the deferred measurement principle. By moving all measurements to the end, we can analyze the circuit using only pure quantum states, without having to consider the effects of intermediate measurements. This simplification makes it easier to reason about the circuit's behavior. Due to the convenience of computing quantum circuits with pure quantum states, we consistently employ the deferred measurement principle for all circuit calculations in this thesis.

2.6 Hadamard Test

The Hadamard test is a quantum algorithmic primitive used to compute the expectation value $\langle\psi|\, U\, |\psi\rangle$, where U is an n-qubit unitary operator and $|\psi\rangle$ is an n-qubit state. Calculating the expectation value of a unitary operator is a fundamental component of many quantum algorithms, such as the Variational Quantum Eigensolver [TCC+22]. More or less surprisingly, we also

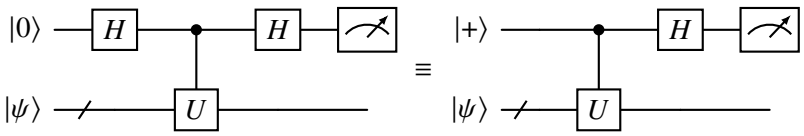

(a) Hadamard test to estimate the real part of $\langle\psi|\, U\, |\psi\rangle$.

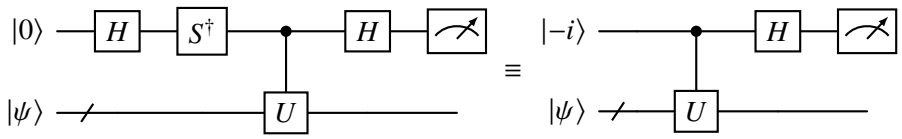

(b) Hadamard test to estimate the imaginary part of $\langle\psi|\, U\, |\psi\rangle$.

Figure 2.6: Hadamard tests to esimate real and imaginary part of $\langle\psi|\, U\, |\psi\rangle$.

encounter the Hadamard test in our research. The Hadamard test uses one ancilla qubit and controlled operations to measure the real and imaginary parts of the expectation value separately. Both variations of the Hadamard test are shown in Figure 2.6. Specifically, the Hadamard test circuit first applies a Hadamard gate to the ancilla qubit, putting it into an equal superposition of $|0\rangle$ and $|1\rangle$. For estimating the imaginary part of $|\psi\rangle$, the Hadamard gate is succeeded by a $S^\dagger$ gate. $S^\dagger$ denotes the complex conjugate of S. It then applies the controlled-U operation, where U acts on the n-qubit state $|\psi\rangle$ conditioned on the state of the ancilla qubit. Finally, another Hadamard gate is applied to the ancilla qubit before measuring it. Note that initializing the ancilla qubits with $|+\rangle$ and $|-i\rangle$, respectively, is equivalent to the operations before the controlled-U gate. The Hadamard test shown in Figure 2.6a then equates to the following state:

$$(H \otimes I)(CU) |+\rangle |\psi\rangle = (H \otimes I) \frac{1}{\sqrt{2}} (|0\rangle |\psi\rangle + |1\rangle U |\psi\rangle) \tag{2.14}$$

$$= \frac{1}{2} (|0\rangle (|\psi\rangle + U |\psi\rangle) + |1\rangle (|\psi\rangle - U |\psi\rangle)) \tag{2.15}$$

$$= |0\rangle \frac{I + U}{2} |\psi\rangle + |1\rangle \frac{I - U}{2} |\psi\rangle \tag{2.16}$$

The probability of measuring the ancilla qubit in the $|0\rangle$ state is $p_r(0) = \frac{1+\mathrm{Re}\langle\psi|U|\psi\rangle}{2}$, allowing the real part of the expectation value to be estimated. Accordingly, the probability of measuring the ancilla qubit in the $|1\rangle$ state is $p_r(1) = 1 - p_r(0) = \frac{1-\mathrm{Re}\langle\psi|U|\psi\rangle}{2}$. Likewise, the measurement probabilities to estimate the imaginary part can be calculated to be $p_i(0) = \frac{1+\mathrm{Im}\langle\psi|U|\psi\rangle}{2}$ and $p_i(1) = \frac{1-\mathrm{Im}\langle\psi|U|\psi\rangle}{2}$. These probabilities are derived from the state:

$$(H \otimes I)(CU) |-i\rangle |\psi\rangle = |0\rangle \frac{I - iU}{2} |\psi\rangle + |1\rangle \frac{I + iU}{2} |\psi\rangle \tag{2.17}$$

Complete calculations are provided in Appendix A.2.

3 Gate Teleportation and Gate Cutting

Entanglement stands as the fundamental resource in quantum teleportation protocols, serving as the linchpin for the faithful transmission of quantum states between distant parties. Traditionally, these protocols rely on maximally entangled states, such as Bell states, shared between the sender and receiver. However, investigating the consequences of deviating from this standard, we examine the impact of NME resource states on gate teleportation. Relaxing the requirement of a maximally entangled state as the shared resource, though feasible, tends to diminish the fidelity of the transmitted quantum states, thereby potentially compromising the reliability and accuracy of the teleportation process.

In the first section of this chapter, we explore the dynamics of the gate teleportation protocol as proposed by Eisert et al. [EJPP00] when employing a NME resource state. Our examination leads to a gate cutting method that establishes a connection between gate teleportation and gate cutting. We then present our improvements, which refine the resulting gate cut. Lastly, relating to the CZ gate decomposition by Mitarai and Fujii [MF21], we show how gate teleportation can mitigate the sampling overhead of gate cutting, albeit requiring an entanglement resource. We provide relevant calculations for our theoretical findings in Appendix A and on GitHub [Hil24].

3.1 Gate Teleportation with NME States

Before we dive into the analysis of gate teleportation with NME resource states, we need to address some technicalities. In the gate teleportation circuit under examination, we defer measurements until the end of the circuit. Adherent to the deferred measurement principle, we can do so without altering the final result of the circuit. This allows us to work with pure states up until the measurements. We depict the circuit in Figure 3.1.

We define $|\tau_{|\phi_{1,2}\rangle}\rangle$ in Equation (3.1) as the pure state obtained when executing the gate teleportation circuit with the resource state $|\phi_{1,2}\rangle$ immediately before the measurements.

$$|\tau_{|\phi_{1,2}\rangle}\rangle := CZ_{2,0}H_2CU_{2,3}CX_{1,2}CX_{0,1}\left(|\phi_{1,2}\rangle\,|\psi_{0,3}\rangle\right) \tag{3.1}$$

Here, $|\psi_{0,3}\rangle$ represents an arbitrary, potentially entangled, two-qubit state, defined by:

$$|\psi\rangle = |\psi_{0,3}\rangle := \begin{bmatrix} a & b & c & d \end{bmatrix}^\top \tag{3.2}$$

where $a, b, c, d \in \mathbb{C}$. And ρ is the corresponding density matrix as defined in Equation (3.3).

$$\rho = |\psi\rangle\,\langle\psi| \tag{3.3}$$

Similarly to Equation (3.1), $\rho_{|\phi_{1,2}\rangle}$ defined in Equation (3.4) denotes the corresponding mixed state post-measurements.

$$\rho_{|\phi_{1,2}\rangle} := \mathrm{Tr}_{0,1}(|\tau_{|\phi_{1,2}\rangle}\rangle\,\langle\tau_{|\phi_{1,2}\rangle}|) \tag{3.4}$$

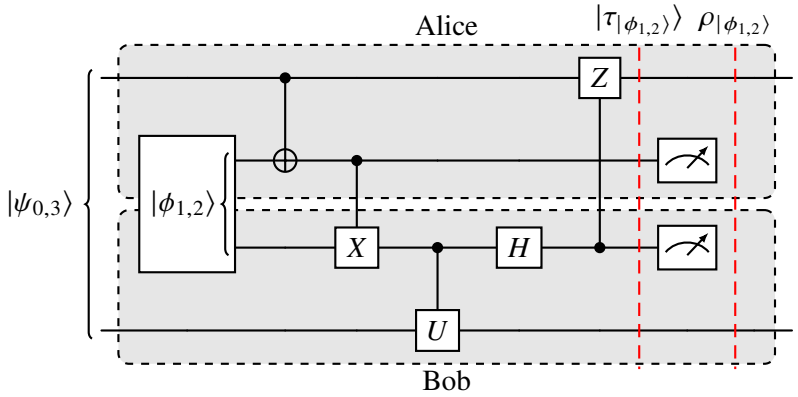

Figure 3.1: Gate teleportation circuit from [EJPP00] with deferred measurements and resource state $|\phi_{1,2}\rangle$.

$\mathrm{Tr}_{1,2}$ denotes the partial trace over qubits 1 and 2. In Figure 3.1, we index the qubits from 0 to 3, arranged from top to bottom. This arrangement enhances readability by visually segregating Alice's and Bob's qubits. However, $|\psi_{0,3}\rangle$ may not be separable, thus we cannot maintain this ordering when expressing the tensor product of $|\phi_{1,2}\rangle$ and $|\psi_{0,3}\rangle$. Consequently, we represent the qubit indices as subscripts in Equations (3.1) and (3.4). From this point onward, we refrain from explicitly writing the indexes, but it is implicit that the resource state is still held by qubits 1 and 2, while the state $|\psi\rangle$ resides on qubits 0 and 3 held by Alice and Bob, respectively. The subscripts of the quantum operations in Equation (3.1) indicate the qubits to which the respective gates are applied. For controlled gates, the first index in the subscript designates the control qubit, while the second index signifies the target qubit. With the notation established, let us examine the gate teleportation circuit using the NME resource state $|\Phi^k\rangle$. We calculate $|\tau_{|\Phi^k\rangle}\rangle$ in Equations (3.5) to (3.10).

$$|\tau_{|\Phi^k\rangle}\rangle = CZ_{2,0}H_2CU_{2,3}CX_{1,2}CX_{0,1}\left(|\Phi^k\rangle|\psi\rangle\right) \tag{3.5}$$

$$= CZ_{2,0}H_2CU_{2,3}CX_{1,2}\left(|\Phi^k\rangle \otimes (a|00\rangle + b|01\rangle) + \frac{(k|01\rangle + |10\rangle) \otimes (c|10\rangle + d|11\rangle)}{\sqrt{k^2+1}}\right) \tag{3.6}$$

$$= CZ_{2,0}H_2CU_{2,3}\left(\frac{(|00\rangle + k|10\rangle) \otimes (a|00\rangle + b|01\rangle) + (k|01\rangle + |11\rangle) \otimes (c|10\rangle + d|11\rangle)}{\sqrt{k^2+1}}\right) \tag{3.7}$$

$$= CZ_{2,0}H_2\left(\frac{(|00\rangle + k|10\rangle) \otimes (a|00\rangle + b|01\rangle)}{\sqrt{k^2+1}} + \frac{(k|01\rangle + |11\rangle) \otimes ((I \otimes U)(c|10\rangle + d|11\rangle))}{\sqrt{k^2+1}}\right) \tag{3.8}$$

$$= CZ_{2,0}\left(\frac{(|0+\rangle + k|1+\rangle) \otimes (a|00\rangle + b|01\rangle)}{\sqrt{k^2+1}} + \frac{(k|0-\rangle + |1-\rangle) \otimes ((I \otimes U)(c|10\rangle + d|11\rangle))}{\sqrt{k^2+1}}\right) \tag{3.9}$$

$$= \frac{(|0+\rangle + k|1+\rangle) \otimes (a|00\rangle + b|01\rangle)(k|0+\rangle + |1+\rangle) \otimes ((I \otimes U)(c|10\rangle + d|11\rangle))}{\sqrt{k^2+1}} \tag{3.10}$$

Next, we compare the resulting density matrices to see how this error manifests after the measurements. For readability we subdivide the the density matrix $\rho_{|\Phi^+\rangle}$ into the 4 submatrices shown in Equations (3.11) to (3.14).

$$\rho_{0,0} = \begin{bmatrix} a\overline{a} & a\overline{b} \\ b\overline{a} & b\overline{b} \end{bmatrix} \tag{3.11}$$

$$\rho_{0,1} = \begin{bmatrix} a\left(\overline{cu_0} + \overline{du_1}\right) & a\left(\overline{cu_2} + \overline{du_3}\right) \\ b\left(\overline{cu_0} + \overline{du_1}\right) & b\left(\overline{cu_2} + \overline{du_3}\right) \end{bmatrix} \tag{3.12}$$

$$\rho_{1,0} = \rho_{0,1}^{\dagger} \tag{3.13}$$

$$\rho_{1,1} = \begin{bmatrix} (cu_0 + du_1)\left(\overline{cu_0} + \overline{du_1}\right) & (cu_0 + du_1)\left(\overline{cu_2} + \overline{du_3}\right) \\ (cu_2 + du_3)\left(\overline{cu_0} + \overline{du_1}\right) & (cu_2 + du_3)\left(\overline{cu_2} + \overline{du_3}\right) \end{bmatrix} \tag{3.14}$$

$\rho_{|\Phi^+\rangle}$ is:

$$\rho_{|\Phi^+\rangle} = \begin{bmatrix} \rho_{0,0} & \rho_{0,1} \\ \rho_{1,0} & \rho_{1,1} \end{bmatrix} \tag{3.15}$$

Remarkably, $\rho_{|\Phi^k\rangle}$ is the same matrix, but with a factor of $\frac{2k}{k^2+1}$ multiplied to the antidiagonal elements. We show this in Equation (3.16).

$$\rho_{|\Phi^k\rangle} = \begin{bmatrix} \rho_{0,0} & \frac{2k}{k^2+1}\rho_{0,1} \\ \frac{2k}{k^2+1}\rho_{1,0} & \rho_{1,1} \end{bmatrix} \tag{3.16}$$

Keep in mind that for $k = 1$ we have the original gate teleportation circuit, which after tracing out the resource state qubits yields exactly $(CU)\,|\psi\rangle\,\langle\psi|\,(CU)^{\dagger}$. However, gate teleportation with a NME resource state does not work error-free, since $\rho_{|\Phi^+\rangle} \neq \rho_{|\Phi^k\rangle}$ for $k \neq 1$. We refer to the error introduced by the NME resource state as E_{nme}. E_{nme} is the difference between $\rho_{|\Phi^+\rangle}$ and $\rho_{|\Phi^k\rangle}$, which we compute in Equation (3.17).

$$E_{nme} := \rho_{|\Phi^+\rangle} - \rho_{|\Phi^k\rangle} = \underbrace{\frac{(k-1)^2}{k^2+1}}_{c} \underbrace{\begin{bmatrix} 0 & \rho_{0,1} \\ \rho_{1,0} & 0 \end{bmatrix}}_{E_\rho} \tag{3.17}$$

The error E_{nme} is composed of the submatrices $\rho_{0,1}, \rho_{1,0}$ on the antidiagonal scaled by a factor of $c := \frac{(k-1)^2}{k^2+1}$ that solely depends on k. We refer to the unscaled error as E_ρ.

To connect the error with the level of entanglement, it is crucial to note that the domain of k is the range $[0, \infty)$, and the degree of entanglement peaks at $k = 1$. That means we need to relate the intervals $[0, 1]$ and $(1, \infty)$ of the error. We achieve this by applying a projective transformation to k: the function $f(x) = \frac{x}{1+x}$ maps the interval from 0 to infinity onto the domain $[0, 1]$. With this transformation, the original interval $[0, 1]$ becomes $[0, 0.5]$, while $(1, \infty)$ is transformed to $(0.5, 1]$. The transformation ensures that the interval $[0, 1]$ and $(1, \infty)$ have the same visual width on a plot. The resulting plot, drawn in Figure 3.2, shows the error weighting factor c with k projectively transformed as described. The plot illustrates that the error decreases as the degree of entanglement increases, and c reaches zero at $k = 1$, where entanglement is maximal. In the absence of entanglement ($k = 0$ and $k \to \infty$), the weighting factor is at its maximum with $c = 1$.

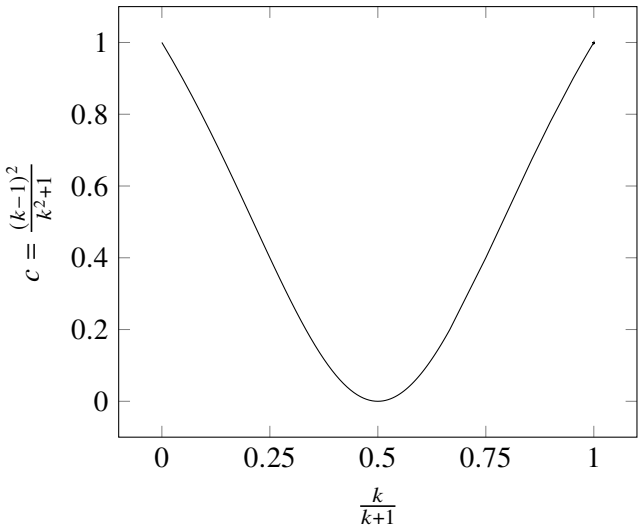

Figure 3.2: Plot of the weighting factor c in the gate teleportation error E_{nme}, where k is projectively transformed by $f(x) = \frac{x}{x+1}$.

In summary, employing NME resource states in the gate teleportation circuit from Eisert et al. [EJPP00] introduces an error in the resulting state. This error amplifies as the degree of entanglement in the utilized resource state decreases. Since the error weighting factor c solely relies on k, it suffices to devise a method to compute the unscaled error E_ρ to achieve error-free gate teleportation, as indicated by Equation 3.18.

$$\rho_{|\Phi^+\rangle} = \rho_{|\Phi^k\rangle} + \underbrace{c \cdot E_\rho}_{E_{nme}} \tag{3.18}$$

We focus on the construction of the unscaled error E_ρ in the following section.

3.2 Gate Cutting with NME Gate Teleportation

In an attempt to identify quantum circuits capable of generating the unscaled teleportation error E_ρ for a NME resource state, we explored the behavior of gate teleportation when initializing the circuit with specific two-qubit states instead of an entangled resource state. The two states that proved successful are $|{+}{+}\rangle$ and $|ii\rangle$. We provide the calculations for relevant resource states, including $|{+}{+}\rangle$ and $|ii\rangle$, in Appendix A.3. It turns out that the error can be broken down into the difference between the final states of the gate teleportation circuit, denoted as $\rho_{|{+}{+}\rangle}$ and $\rho_{|ii\rangle}$ when employing $|{+}{+}\rangle$ and $|ii\rangle$ as resource states. We express this equivalence in Equation Equation (3.19).

$$E_\rho = \rho_{|{+}{+}\rangle} - \rho_{|ii\rangle} \tag{3.19}$$

The calculations for Equation (3.19) can be found in Appendix A.3

The decomposition of E_ρ into $\rho_{|{+}{+}\rangle}$ and $\rho_{|ii\rangle}$ facilitates an error-correcting implementation of gate teleportation with NME states by executing the same quantum circuit with different initializations. Precisely, Equation (3.19) allows us to cut an arbitrarily controlled gate CU by evaluating the gate teleportation circuit with three different resource states as shown in Figure 3.3. On the left side, the

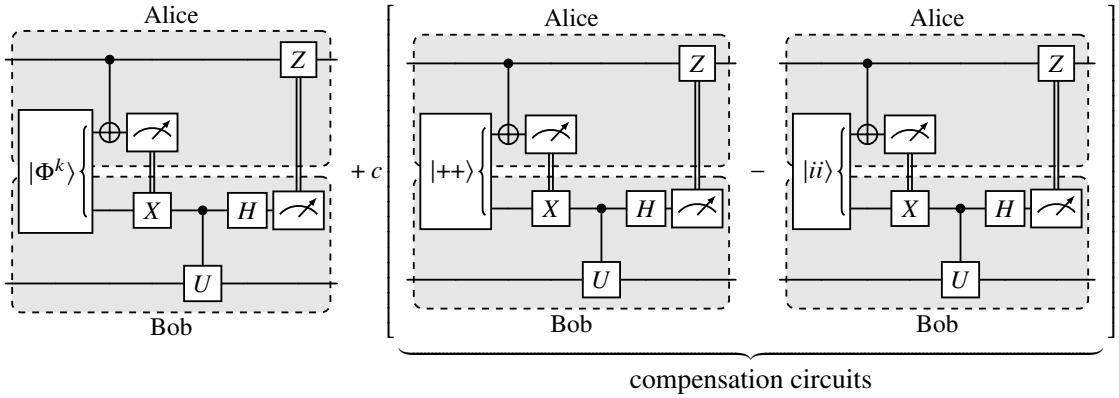

Figure 3.3: Gate cut of a controlled gate with NME gate teleportation.

gate teleportation circuit utilizing the NME resource state to compute $\rho_{|\Phi^k\rangle}$ can be seen. This circuit introduces the error E_{nme}, of which the circuit diverges from the original gate teleportation circuit. E_{nme} is broken down into the scaling factor c and the error matrix E_ρ, which is further decomposed as per Equation (3.19). E_{nme} is computed by the remaining part of Figure 3.3 including the two circuits that compute $\rho_{|{+}{+}\rangle}$ and $\rho_{|ii\rangle}$ to which we from now on refer to as compensation circuits. We state the gate cut mathematically in Equation (3.20).

$$\rho_{|\Phi^+\rangle} = \rho_{|\Phi^k\rangle} + \underbrace{c\left(\rho_{|{+}{+}\rangle} - \rho_{|ii\rangle}\right)}_{E_{nme}} \tag{3.20}$$

Notably, the compensation circuits do not require an entangled resource state, Alice and Bob just have an ancilla qubit each. Therefore, the compensation circuits do not increase the required resources entanglement-wise. To cut a controlled quantum gate CU that acts on two qubits, we need to replace CU with the gate teleportation circuit, which uses the resource state $|\Phi^k\rangle$. To counteract the error introduced by the NME resource state, we must also run the compensation circuits. To maintain the same error rate as the non-cut circuit, the circuit with the NME gate teleportation must be executed with the same number of shots, and each compensation circuit needs to be run c times this number. Consequently, using NME resource states incurs a sampling overhead of $1 + 2c$. When $k = 1$, there is no additional sampling overhead, as the compensation circuits are not needed. However, as the degree of entanglement decreases, the sampling overhead increases. Ultimately, when there is no entanglement, both compensation circuits must be executed as many times as the NME gate teleportation circuit to maintain the same statistical accuracy. This is the worst-case scenario, resulting in a total sampling overhead of 3.

Another discovery we have made is that applying the Pauli-Z gate to both ancilla qubits within the compensation circuits does not alter their final states. Applying the Pauli-Z gate to both ancilla qubits equates to initializing the ancilla qubits to the states $|{-}{-}\rangle$ and $|{-}i\,{-}\,i\rangle$, respectively (refer to Appendix A.3). We state the equivalence of the final states in Equations (3.21) and (3.22).

$$\rho_{|{+}{+}\rangle} = \rho_{|{-}{-}\rangle} \tag{3.21}$$

$$\rho_{|ii\rangle} = \rho_{|{-}i{-}i\rangle} \tag{3.22}$$

This implies that the respective circuits can be used interchangeably without affecting the result.

3.3 Improving the Compensation Circuits

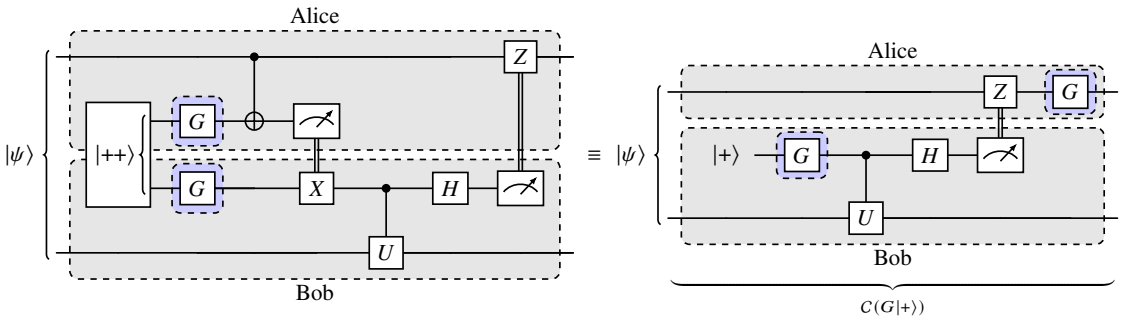

Figure 3.4: Elimination of Alice's ancilla qubit where $G = \begin{bmatrix} g & 0 \\ 0 & e^{i\varphi}\overline{g} \end{bmatrix}$ is unitary and $g^4 = e^{4i\varphi}\overline{g}^4$.

Figure 3.3 provides a gate cut that accommodates varying degrees of entanglement in the resource state, offering a trade-off between reduced entanglement and increased sampling overhead. In this section, we demonstrate that the compensation circuits can be improved. Specifically, Alice's ancilla qubit can be removed making the compensation circuits more resource efficient. To validate this simplification, we establish the equivalence illustrated in Figure 3.4 by considering a unitary matrix G as defined in Equation (3.23).

$$G := \begin{bmatrix} g & 0 \\ 0 & e^{i\varphi}\overline{g} \end{bmatrix} \tag{3.23}$$

where $\varphi \in \mathbb{R}, g \in \mathbb{C}, |g| = 1$ and $\overline{g}$ is the complex conjugate of g. G is unitary since $GG^\dagger = I$ and the formulation of G includes the quantum gates I, Z, S and $S^\dagger$. The corresponding values of g and φ are shown in Equations (3.24) to (3.27) where $n \in \mathbb{Z}$.

$$G = I \iff g = 1, \varphi = 2\pi n \tag{3.24}$$
$$G = Z \iff g = 1, \varphi = 2\pi n + \pi \tag{3.25}$$
$$G = S \iff g = 1, \varphi = 2\pi n + \frac{\pi}{2} \tag{3.26}$$
$$G = S^\dagger \iff g = 1, \varphi = 2\pi n - \frac{\pi}{2} \tag{3.27}$$

We denote the improved circuit as $C(|\phi\rangle)$ where Bob's ancilla qubit is initialized to $|\phi\rangle$.

For convenience, we define a shorthand notation for the final state before and after measurement of the improved circuit in a similar manner to Equations (3.1) and (3.4) in Equations (3.28) and (3.29).

$$|\tau'_G\rangle := G_1 CZ_{0,1} H_0 CU_{0,2} G_0 \left(|+\rangle |\psi\rangle\right) \tag{3.28}$$
$$\rho'_G := \mathrm{Tr}_0(|\tau'_G\rangle \langle\tau'_G|) \tag{3.29}$$

We base the definitions of $|\tau'_G\rangle$ and ρ'_G on the circuit with a deferred measurement shown in Figure 3.5.

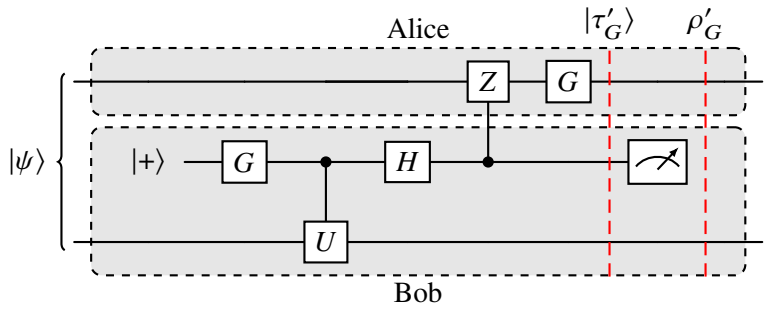

Figure 3.5: Improved compensation circuit $C(G\,|+\rangle)$ with deferred measurement.

To establish a criterion for G such that $\rho'_G = \rho_{(G\otimes G)|{+}{+}\rangle}$, we analyze the disparity between the two density matrices. This disparity must be equal to the zero matrix for $\rho'_G = \rho_{(G\otimes G)|{+}{+}\rangle}$. The expression for $\rho'_G - \rho_{(G\otimes G)|{+}{+}\rangle}$ is presented in Equation (3.30).

$$\rho'_G - \rho_{(G\otimes G)|{+}{+}\rangle} = \frac{1}{4}\left(g^4 - e^{4i\varphi}\overline{g}^4\right) e^{-2i\varphi} \begin{bmatrix} 0 & E_T \\ -E_T^\dagger & 0 \end{bmatrix} \tag{3.30}$$

where E_T is defined in Equation (3.31).

$$E_T = \begin{bmatrix} a\left(\overline{cu_0} + \overline{d}\overline{u_1}\right) & a\left(\overline{cu_2} + \overline{d}\overline{u_3}\right) \\ b\left(\overline{cu_0} + \overline{d}\overline{u_1}\right) & b\left(\overline{cu_2} + \overline{d}\overline{u_3}\right) \end{bmatrix} \tag{3.31}$$

We provide the calculations for $\rho_{(G\otimes G)|{+}{+}\rangle}$ and ρ'_G in Appendix A.4.

Since $e^{-2i\varphi} \neq 0$, Equation (3.30) yields one condition depending on the parameters g and φ such that the equivalence of Figure 3.4 holds true. This condition stipulates that the multiplication factor, which depends on g, must be equal to 0, as illustrated in Equation (3.32).

$$g^4 - e^{4i\varphi}\overline{g}^4 \stackrel{!}{=} 0 \tag{3.32}$$

Remarkably, $G \in \{I, Z, S, S^\dagger\}$ satisfies Equation (3.32). We can therefore eliminate Alice's ancilla qubit in the compensation circuits because of the equivalences of the respective final states depicted in Equations (3.33) to (3.36).

$$\rho_{|{+}{+}\rangle} = \rho'_I \tag{3.33}$$
$$\rho_{|{-}{-}\rangle} = \rho'_Z \tag{3.34}$$
$$\rho_{|ii\rangle} = \rho'_S \tag{3.35}$$
$$\rho_{|{-}i{-}i\rangle} = \rho'_{S^\dagger} \tag{3.36}$$

By eliminating Alice's ancilla qubit, the number of qubits required in the compensation circuits is reduced to three, while the classical communication is reduced to just one bit. Previously, Alice had to send the measurement outcome of her ancilla qubit to Bob, but this is no longer necessary in the improved circuit. The resulting controlled gate decomposition refines the expression from Equation (3.20) as shown by Equation (3.37).

$$\rho_{|\Phi^+\rangle} = \rho_{|\Phi^k\rangle} + c\left(\rho'_I - \rho'_S\right) \tag{3.37}$$

The sampling overhead of the gate cut with improved compensation circuits remains $1 + 2c$ since the compensation circuits are not further decomposed. Unfortunately, the improved compensation circuits still require Bob to use an ancilla qubit and one bit of classical communication to transmit the measurement of this ancilla qubit to Alice. We address these issues in the next section.

3.4 Decomposing the Compensation Circuits

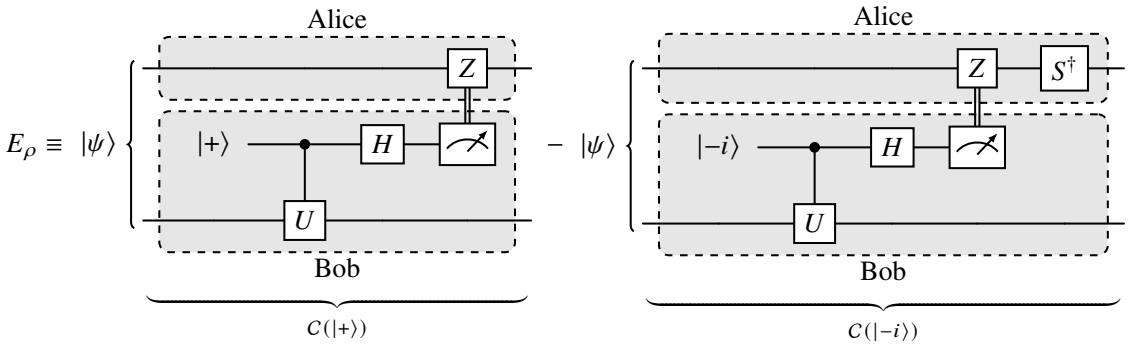

Figure 3.6: Error E_ρ: Compensation circuits where Alice's ancilla qubit is eliminated and Bob performs Hadamard tests.

In this section, we aim to eliminate Bob's ancilla qubit and the remaining bit of classical communication from the improved compensation circuits depicted in Figure 3.6. We have identified two almost identical decompositions for these circuits, which are detailed in the following subsections. In figures illustrating circuit decompositions involving two qubits, the upper qubit belongs to Alice and the lower qubit belongs to Bob even if it is not explicitly indicated. We end this section by comparing the sampling overheads of the decompositions presented in this chapter.

3.4.1 Hadamard Test-Based Decomposition

There is an intriguing aspect to Bob's portion of the improved compensation circuits: if we construct E_ρ from ρ'_I and $\rho'_{S^\dagger}$, Bob performs the Hadamard test in both circuits and communicates the ancilla qubit's measurement result to Alice. In ρ'_I, Bob uses the Hadamard test for the real component of $\langle\psi| U |\psi\rangle$ (Figure 2.6a), and in $\rho'_{S^\dagger}$, he applies the Hadamard test for the imaginary component (Figure 2.6b). The circuits for this are shown in Figure 3.6.

Recall from Equations (2.16) and (2.17) that after Bob applies the Hadamard tests in $C(|+\rangle)$ and $C(|-i\rangle)$, his qubits are in the states $|0\rangle \frac{I+U}{2} |\psi_B\rangle + |1\rangle \frac{I-U}{2} |\psi_B\rangle$ and $|0\rangle \frac{I-iU}{2} |\psi_B\rangle + |1\rangle \frac{I+iU}{2} |\psi_B\rangle$, respectively. Here, $|\psi_B\rangle$ represents the state held by Bob's qubit. Given that Alice applies the Z gate on her qubit only when Bob's ancilla qubit is in state $|1\rangle$, we can express the respective states as shown in Equations (3.38) and (3.39).

$$|\tau'_I\rangle = |0\rangle \otimes \left(I \otimes \frac{I+U}{2}\right) |\psi\rangle + |1\rangle \otimes \left(Z \otimes \frac{I-U}{2}\right) |\psi\rangle \tag{3.38}$$

$$|\tau'_{S^\dagger}\rangle = |0\rangle \otimes \left(S^\dagger \otimes \frac{I-iU}{2}\right) |\psi\rangle + |1\rangle \otimes \left(S \otimes \frac{I+iU}{2}\right) |\psi\rangle \tag{3.39}$$

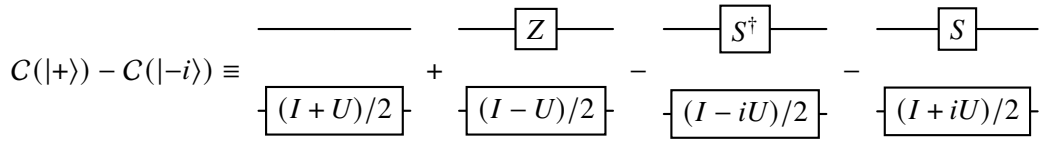

Figure 3.7: Decomposition of the compensation circuits $C(|+\rangle)$ and $C(|-i\rangle)$.

Tracing out Bob's ancilla qubit, as it is measured, results in the density matrices shown in Equations (3.40) and (3.41).

$$\rho'_I = \left(I \otimes \frac{I+U}{2}\right) \rho \left(I \otimes \frac{I+U}{2}\right)^\dagger + \left(Z \otimes \frac{I-U}{2}\right) \rho \left(Z \otimes \frac{I-U}{2}\right)^\dagger \tag{3.40}$$

$$\rho'_{S^\dagger} = \left(S^\dagger \otimes \frac{I-iU}{2}\right) \rho \left(S^\dagger \otimes \frac{I-iU}{2}\right)^\dagger + \left(S \otimes \frac{I+iU}{2}\right) \rho \left(S \otimes \frac{I+iU}{2}\right)^\dagger \tag{3.41}$$

This facilitates the decomposition $E_\rho = \rho'_I - \rho'_{S^\dagger}$. The corresponding circuit decomposition is shown in Figure 3.7.

The operations $\frac{I \pm U}{2}$ and $\frac{I \pm iU}{2}$, that Bob has to apply to his qubit, are not necessarily unitary and therefore cannot be directly implemented as quantum gates. Implementing non-unitary operations on quantum computers typically requires additional resources such as additional ancilla qubits [DK17; SHS+22]. We show how a subset of these gates can be implemented when U is hermitian ($U = U^\dagger$). Notably, the gates X, Y, Z, and H are hermitian.

First, we establish a useful property of unitary matrices. Any 2×2 matrix U that is unitary can be diagonalized by another matrix $V \in \mathbb{C}^{2\times 2}$ such that $U = V\Lambda V^{-1}$ [HJ85]. Here, V is the matrix whose columns are the eigenvectors v_1, v_2 of U corresponding to the eigenvalues λ_1 and λ_2, and

$$\Lambda = \operatorname{diag}(\lambda_1, \lambda_2) = \begin{bmatrix} \lambda_1 & 0 \\ 0 & \lambda_2 \end{bmatrix} \tag{3.42}$$

is a diagonal matrix with its diagonal elements being the eigenvalues of U. This decomposition is referred to as the eigendecomposition. Fortunately, if v_1 and v_2 are normalized, V becomes unitary, which is a characteristic of Hermitian matrices. This stems from the fact that the normalized eigenvectors of hermitian matrices are orthonormal, meaning $\langle v_i, v_i \rangle = 1$ for $i \in \{0, 1\}$ and $\langle v_1, v_2 \rangle = 0$ [HJ85]. Thus, we can assume $V^{-1} = V^\dagger$. When we use the eigendecomposition of U in the operations Bob has to apply, we can reformulate them according to Equation (3.43).

$$\frac{I \pm i^b U}{2} = \frac{I \pm V i^b \Lambda V^\dagger}{2} = \frac{VIV^\dagger \pm V i^b \Lambda V^\dagger}{2} = V \left(\frac{I \pm i^b \Lambda}{2}\right) V^\dagger \tag{3.43}$$

In Equation (3.43) $b \in \{0, 1\}$ distinguishes the gates from $C(|+\rangle)$ ($b = 0$) and $C(|-i\rangle)$ ($b = 1$). Reformulating Bob's gates in this manner moves us closer to a decomposition that can be implemented on a quantum computer. Since V and $V^\dagger$ are unitary, they can be realized as quantum gates, leaving us with the task of handling $\frac{I \pm i^b \Lambda}{2}$. Additionally, we note that matrices that are both unitary and hermitian have eigenvalues of ± 1. This is because eigenvalues of unitaries have absolute value 1 and eigenvalues of hermitians are real [Axl24; HJ85]. Consequently, in the eigendecomposition of

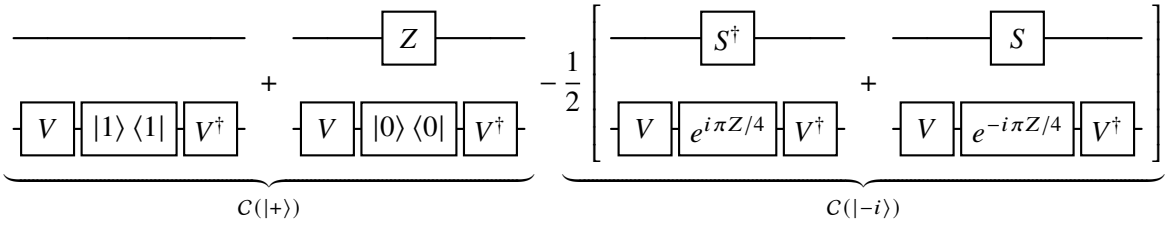

Figure 3.8: Decomposition of the compensation circuits $C(|+\rangle)$ and $C(|-i\rangle)$ for hermitian unitaries.

$U, \lambda_1, \lambda_2 \in \{-1, 1\}$, which implies that Λ is either $\pm I$ or $\pm Z$. These four instances can be simplified to the scenario where $\Lambda = -Z$. When $\Lambda \pm I$, it results in $U = V\Lambda V^\dagger = \pm I$, as V is unitary. The case $U = I$ is irrelevant because a controlled identity gate can be eliminated by simply removing it. When $U = -I$, CU can be written as tensor product $CI = I \oplus (-I) = Z \otimes I$, and therefore, no cut is needed. $\Lambda = \pm Z$ is only possible if U has eigenvalues 1 and -1. Then we can freely choose which eigenvalue we declare as λ_1 and λ_2. V must be constructed accordingly. Without loss of generality, we can always choose $\lambda_1 = -1$ and $\lambda_2 = 1$ which implies $\Lambda = -Z$. Following this reasoning, we could also assume $\Lambda = Z$, but choosing $\Lambda = -Z$ makes this section better comparable to Section 3.4.2. The operations Bob has to perform are outlined in Equations (3.44) to (3.47).

$$\frac{I+Z}{2} = \begin{bmatrix} 1 & 0 \\ 0 & 0 \end{bmatrix} = |0\rangle\langle 0| \tag{3.44}$$

$$\frac{I-Z}{2} = \begin{bmatrix} 0 & 0 \\ 0 & 1 \end{bmatrix} = |1\rangle\langle 1| \tag{3.45}$$

$$\frac{I+iZ}{2} = \frac{e^{i\pi Z/4}}{\sqrt{2}} \tag{3.46}$$

$$\frac{I-iZ}{2} = \frac{e^{-i\pi Z/4}}{\sqrt{2}} \tag{3.47}$$

The operations represented by $|0\rangle\langle 0|$ and $|1\rangle\langle 1|$ are the projection matrices for Z-basis measurements. These can be realized through projective measurements. When Bob needs to compute $|0\rangle\langle 0|$ on his qubit, he measures the qubit and ensures it is in the state $|0\rangle$. Should Bob measure $|0\rangle$, he proceeds with the computation. If he measures $|1\rangle$, he applies an X gate to his state, converting it to $|0\rangle$ before proceeding with the computation. Applying $|1\rangle\langle 1|$ works analogously.

The operation $e^{\pm i\pi Z/4}$ from Equations (3.46) and (3.47) are unitary and allow us to rewrite Equation (3.41) to Equation (3.48).

$$\begin{aligned} \rho'_{S^\dagger} = \frac{1}{2}\Bigg(&\left(S^\dagger \otimes \left(Ve^{i\pi Z/4}V^\dagger\right)\right)\rho\left(S^\dagger \otimes \left(Ve^{i\pi Z/4}V^\dagger\right)\right)^\dagger \\ &+ \left(S \otimes \left(Ve^{-i\pi Z/4}V^\dagger\right)\right)\rho\left(S \otimes \left(Ve^{-i\pi Z/4}V^\dagger\right)\right)^\dagger \Bigg) \end{aligned} \tag{3.48}$$

Given, that we can realize all operations from Equations (3.44) to (3.47), we can compose the compensation circuits as shown in Figure 3.8 according to Equation (3.48) for hermitian operators U. This decomposition requires no ancilla qubits and no classical communication. However, it

comes at the cost of increasing the sampling overhead compared to the original compensation circuit decomposition. For the decomposition of hermitian operators shown in Figure 3.8, each compensation circuit is divided into two smaller circuits, two of which are weighted by 1 and two which are weighted by $\frac{1}{2}$. Consequently, an overall gate cut with NME gate teleportation using the decompositions from Figure 3.7 results in a sampling overhead of $1 + 3c$. The gate teleportation circuit with NME resource state is weighted with 1 and the decomposition from Figure 3.7 is weighted by c.

3.4.2 Decomposition for the Controlled-{X, Y, Z, H} Gate

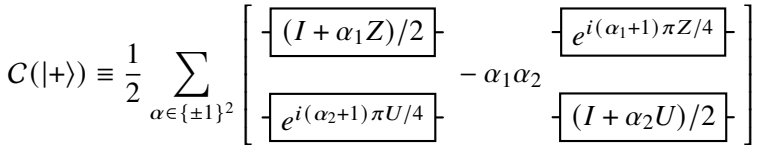

(a) Decomposition of the compensation circuit $C(|+\rangle)$.

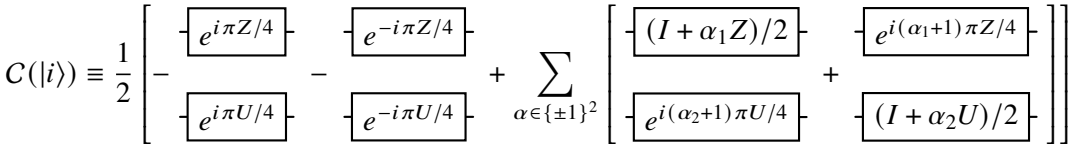

(b) Decomposition of of the compensation circuit $C(|i\rangle)$.

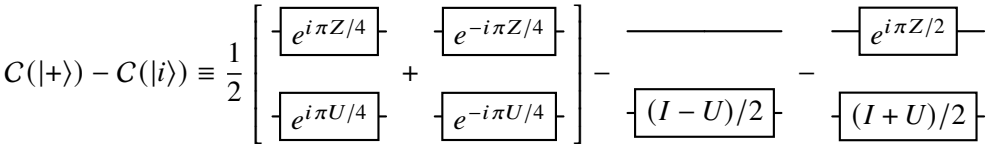

(c) Decomposition of the circuit for E_ρ: $C(|+\rangle) - C(|i\rangle)$.

Figure 3.9: Decomposition of the compensation circuits similar to the CZ decomposition of Mitarai and Fujii [MF21] for $U \in \{X, Y, Z, H\}$.

In our effort to eliminate Bob's ancilla qubit and the remaining classical communication from the improved compensation circuits from Figure 3.6, we discovered a decomposition that is almost identical to the one from the previous section. As a starting point, we used the CZ gate decomposition from Mitarai and Fujii [MF21]. Our investigation extends to evaluating whether the compensation circuits $C(|+\rangle)$ and $C(|i\rangle)$ can undergo a similar decomposition as depicted in Figure 2.4. Our findings reveal that indeed they can. Shown in Figures 3.9a and 3.9b are the decompositions for $C(|+\rangle)$ and $C(|i\rangle)$, respectively. All circuits in the decompositions stem from the decomposition of Mitarai and Fujii [MF21]. It is important to note that these decompositions are not universally applicable to all controlled gates. However, the decomposition is valid for the controlled-{X, Y, Z, H} gates. The corresponding calculations are provided in Appendix A.5.

The decomposition of $C(|+\rangle)$ comprises eight circuits, while that of $C(|i\rangle)$ encompasses 10 circuits, each with a weighting factor of $\frac{1}{2}$. To obtain a decomposition of the unscaled NME gate teleportation error E_ρ, we subtract these decompositions from each other, as depicted in Figure 3.9. The advantage we get from this combined decomposition is that most of the circuits nullify each other. Consequently, we are left with four circuits with the weighting factors $\frac{1}{2} + \frac{1}{2} + 1 + 1 = 3$, resulting in a sampling overhead of $3c$ for E_{nme}. While a sampling overhead of $3c$ surpasses the overhead of $2c$ discussed in the previous section (refer to Equation 3.20), the decomposition from Figure 3.9 does not necessitate any ancilla qubits, optimizing the number of required qubits.

When comparing the two decompositions from Figures 3.8 and 3.9c, we observe that both consist of four circuits with the same weighting factors. Although the weighting factors differ in their sign, this difference can be eliminated by multiplying one of the decompositions by -1. The similarities between the two decompositions are striking. The gates Alice performs in both decompositions are essentially the same, apart from a multiplication factor. This can be seen from the equivalences in Equations (3.49) to (3.51).

$$e^{i\pi Z/2} = iZ \tag{3.49}$$

$$e^{i\pi Z/4} = e^{i\pi/4} S^\dagger \tag{3.50}$$

$$e^{-i\pi Z/4} = e^{-i\pi/4} S \tag{3.51}$$

When comparing the gates Bob executes on his qubit, we notice that in Figure 3.8, he performs $V\frac{I-Z}{2}V^\dagger$, which corresponds to $\frac{I-U}{2}$ in the corresponding circuit from Figure 3.9c. Similarly, $V\frac{I+Z}{2}V^\dagger$ corresponds to $\frac{I+U}{2}$. In Figure 3.7, these operations appear switched, but this is due to our previous choice of $\Lambda = -Z$, which changes the signs accordingly. In circuits with a weighting factor of $\frac{1}{2}$, the signs in front of the Z and U gates also match. Specifically, $Ve^{\pm i\pi Z/4}V^\dagger$ corresponds to $e^{\pm i\pi U/4}$. The similarity between the two decompositions underscores their validity, which we have confirmed for Figure 3.9c through calculations for the controlled X, Y, Z, and H gates (refer to Appendix A.5).

To conclude this part, we look at the sampling overhead of the gate cut the error decomposition from Figure 3.9c facilitates. To cut a controlled X, Y, Z, or H gate, the controlled gate teleportation circuit must be executed by adding 1 to the sampling overhead of $3c$. The decomposition we present in this section enables reducing the sampling overhead of the controlled gate decomposition from Mitarai and Fujii [MF21] from 5 to $1 + 3c$, albeit at the expense of an entangled resource state. In the worst-case scenario, where no entangled resource state is available, the sampling overhead is $1 + 3c \overset{c=1}{=} 4$. Although our decomposition enhances the sampling overhead, it requires two extra qubits and two bits of classical communication for the NME gate teleportation circuit. Nonetheless, the sampling overhead can be reduced by taking advantage of the use of NME states compared to the decomposition of Mitarai and Fujii [MF21].

3.4.3 Sampling Overhead Comparison

In this chapter, we presented three distinct decompositions for compensating the error introduced by a NME resource state in the gate teleportation circuit from Eisert et al. [EJPP00]. These decompositions are depicted in Figures 3.6, 3.8 and 3.9c, each equating to $C(|+\rangle) - C(|-i\rangle)$. All three decompositions come with their drawbacks. We now focus on one of these drawbacks: the sampling overhead. For simplicity, we only consider the sampling overhead of the weighted error

E_{nme}. To obtain the overall sampling overhead for the corresponding gate cut, one would need to add 1 to the sampling overheads. The error decomposition utilizing the improved compensation circuits has a sampling overhead of $2c$. The decompositions shown in Figures 3.8 and 3.9c result in a sampling overhead of $3c$. The sampling overheads are plotted in Figure 3.10.

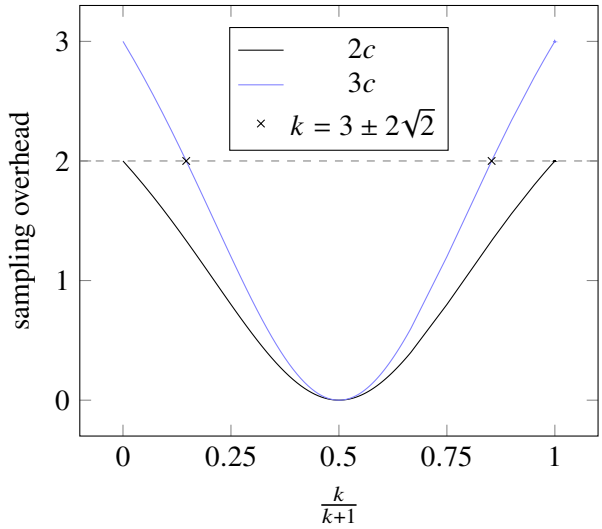

Figure 3.10: Comparison of the sampling overheads $2c$ and $3c$ of the error decompositions in Figures 3.6, 3.7 and 3.9c. The degree of entanglement k is projectively transformed by $f(x) = \frac{x}{x+1}$.

As can be seen, the difference in sampling overheads decreases with higher degrees of entanglement and increases with lesser degrees. The sampling overhead of $2c$ is smaller for all k values except for $k = 1$, where the sampling overhead is 0 for all decompositions. However, we can achieve an advantage with the latter two decompositions over the first approach without entanglement. Setting $c = 1$ for the improved compensation circuits, we obtain a sampling overhead of 2. So the question is for which k the sampling overhead of $3c$ is equal to 2. The respective k value is expressed in Equation (3.52).

$$\underbrace{3\,\frac{(k-1)^2}{k^2+1}}_{c} = 2 \iff k = 3 \pm 2\sqrt{2} \tag{3.52}$$

Equation (3.52) implies that the gate cut facilitated by the decomposition from Figures 3.8 and 3.9c provides an advantage for k in the interval $\in \left(3 - 2\sqrt{2}, 3 + 2\sqrt{2}\right)$ compared to the basline approach facilitated by Figure 3.6.

4 Experiments

This section presents a numerical demonstration highlighting the benefits of using NME states in the gate cutting process. Our experimental setup applies the gate cut from Section 3.2 with improved compensation circuits to random controlled gates for various degrees of entanglement. The goal is to verify the correlation between the degree of entanglement in the resource state and the incurred sampling overhead, as described in Chapter 3. We use the open-source SDK Qiskit for working with quantum computers, implemented in Python [JTK+24].

Our setup for a single gate cut is as follows: We choose a random initial two-qubit quantum state $|\psi\rangle$ and a random 2×2 unitary U. From U, we create a controlled gate $CU = I \oplus U$ that we want to teleport. Next, we create the gate teleportation circuit from Figure 2.2 with CU and the corresponding two compensation circuits $C(|+\rangle)$ and $C(|i\rangle)$. We then run the circuits for different values of $k \in \{0, 5 - 2\sqrt{6}, \frac{5-\sqrt{21}}{2}, \frac{1}{3}, \frac{1}{2}, 1\}$ and measure the qubits that initially hold the state $|\psi\rangle$. These specific k values lie equidistantly in the range of possible sampling overhead values, as illustrated in Figure 4.1. We choose k values from the interval $[0, 1]$ since values from $[1, \infty)$ would yield symmetrical c values. For every $k \leq 1$, there exists a $k \geq 1$ that yields the same c value and therefore the same sampling overhead.

We run the gate teleportation circuit with NME resource state for 5000 shots and the compensation circuits depending on the respective k value c times. To inspect the error in relation to the number of shots, we take increasingly many samples from the executions and compute the L_2-norm between

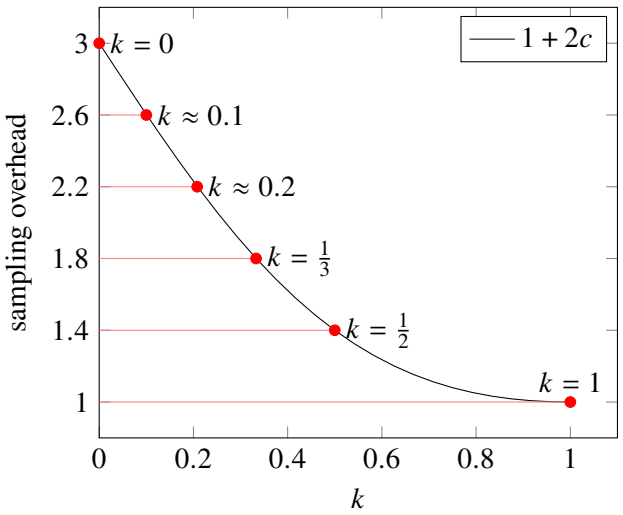

Figure 4.1: Plot of the sampling overhead $1 + 2c$ for the gate cut from Figure 3.3 with improved compensation circuits for $k \in [0, 1]$. Six equidistant sampling overhead values for $k \in \{0, 5 - 2\sqrt{6}, \frac{5-\sqrt{21}}{2}, \frac{1}{3}, \frac{1}{2}, 1\}$ are highlighted.

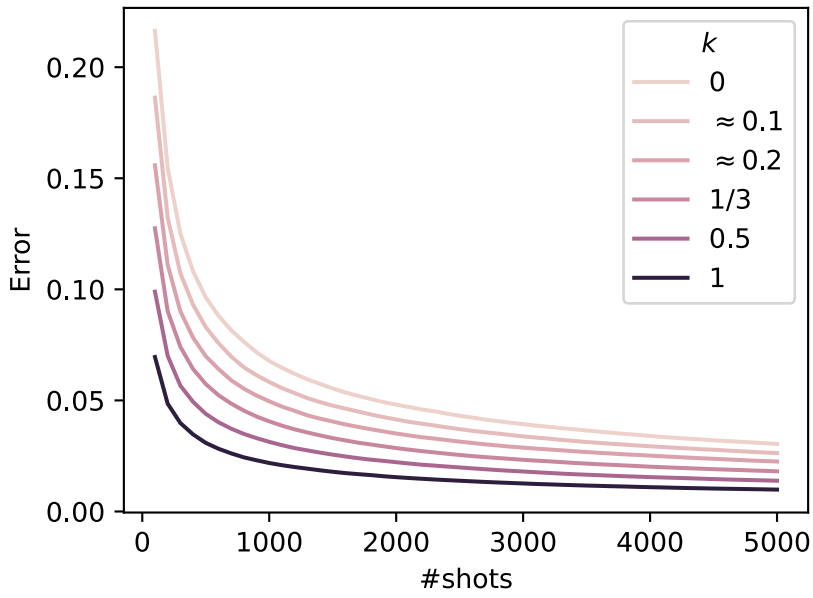

Figure 4.2: Average L_2-norm between the gate cut from Section 3.2 and the expected result for different degrees of entanglement in the resource state.

the true and sampled probabilities. Starting with approximately $n = 100$ overall samples. The number of shots sampled is not always exactly n because 100 id not divisible by $1 + 2c$ for all c values. We actually sample n_{tp} times the gate teleportation and n_{comp} times each compensation circuit with $n \approx n_{tp} + n_{comp}$. The general forms of n_{tp} and n_{comp} are shown in Equations (4.1) and (4.2).

$$n_{tp} = \left\lfloor \frac{n}{1 + 2c} \right\rfloor \tag{4.1}$$

$$n_{comp} = c \cdot n_{tp} \tag{4.2}$$

We compute the sampled probabilities for each n by dividing the count of each measurement outcome by the number of samples $n_{tp} + n_{comp}$. We then calculate the error as the L_2-norm of the difference between the sampled probabilities and the true probabilities. This process is repeated, increasing n by 100 until reaching $n = 5000$.

We repeat this procedure 1000 times for 10 different random combinations of $|\psi\rangle$ and U each, and average the error. The average error in relation to the number of shots for different k values is plotted in Figure 4.2. The results illustrate a clear relationship between the degree of entanglement of the resource state and the deviation from the exact result for the same number of overall shots. Our findings are consistent with the theoretical insights presented in Chapter 3 regarding the sampling overhead. Additionally, we observe that higher degrees of entanglement lead to faster convergence in the number of shots. When $k = 1$, serving as a baseline with the original gate teleportation, no shots are allocated to the compensation circuits, and deviations from the exact result arise solely from statistical errors due to the finite number of shots. Conversely, when $k = 0$, a gate cut without any entanglement resource results in a larger sampling overhead. The error curves are evenly spaced due to our choice of k values. Overall, these observations reinforce the theoretical considerations discussed in Chapter 3.

5 Discussion

In this chapter, we address the significance of our research and its contributions to quantum computing. We initially frame our discussion by examining the gate cut identified in Figure 3.3. This gate cut enables cutting controlled two-qubit quantum gates, excluding gates with an operator Schmidt rank of 4.

The value of this gate cut emerges in scenarios where circuit cutting is essential for practical quantum computation, e.g. due to hardware limitations, and where entanglement distribution between distant quantum computers is feasible but imperfect. For example, it may be more practical to distribute NME qubit pairs instead of maximally entangled ones due to noisy hardware. In such settings, gate cutting via NME resource states would be advantageous. This scenario is conceivable in the near future, given that decoherence and limited quantum hardware are major challenges in quantum computing research [CTV17; GPAY23; MK13; Pre18]. However, since no reliable and cost-effective method for the entanglement distribution has been established yet, our research currently holds more theoretical significance [AAS23; KMSD19].

Our proposed gate cutting technique interpolates between gate teleportation and gate cutting, mitigating the respective disadvantages of requiring entanglement and incurring sampling overhead. We avoid quantifying the relationship between entanglement and sampling overhead because it only makes sense within the context of the specific definition of NME states and the entanglement quantification measure employed. Depending on these factors, the relationship can exhibit different mathematical forms, potentially quadratic or trigonometric. But we can compare the relation to other research. This research aligns closely with that of Bechtold et al. [BBLM23], who explored the connection between quantum teleportation and wire cutting. Remarkably, the circuit decomposition Bechtold et al. [BBLM23] present, involves the quantum teleportation circuit and two compensation circuits each weighted by a factor. Precisely, the NME resource state incurred error, and the circuit decomposition from Bechtold et al. [BBLM23] suggest parallels that indicate the potential for transferring research results between these methods.

Our proposed gate cut (Figure 3.3) can be expanded to accommodate multi-controlled U gates through iterative application. Building upon the work of Eisert et al. [EJPP00], Sarvaghad-Moghaddam and Zomorodi [SZ21] have shown that the gate teleportation circuit, which serves as the foundation of our investigation, is extendable to multi-party multi-controlled U gates. This extension involves establishing shared Bell pairs between the party possessing the target qubit and each control qubit holder. Subsequently, the teleportation circuit is executed between each control party and the target party. The U gate on the target party is then collectively controlled by all qubits participating in the shared Bell pairs on the target party. The target party can add additional control qubits as well. The extension of our gate cut methodology mirrors the approach of multi-party multi-controlled gate teleportation. Each application of the gate cut can be interpreted as dividing the circuit between the target party and an additional control party. Resource considerations for each cut include the need for an extra shared NME state and at least two and at most four bits of

classical communication. Specifically, each execution of the gate teleportation circuit requires two bits of classical communication, wherein Alice and Bob exchange their measurement outcomes. For each execution of an improved compensation circuit, Bob must send one bit to Alice, informing her of the measurement outcome of his ancilla qubit. For maximally entangled resource states the execution of the compensation circuits is omitted, reducing the classical communication to only two bits per execution. The associated sampling overhead scales with the number of control qubits ($O((2c)^n)$), which is the same for cutting multiple two-qubit controlled gates.

In our efforts to improve the compensation circuits, we discovered the circuit simplification depicted in Figure 3.4. Although we require this simplification only for $G \in \{I, Z, S, S^\dagger\}$, we proved that it works for a broader range of gates (refer to Equations (3.23) and (3.32)). An interesting observation from our research is that the improved compensation circuits incorporate the Hadamard test. The Hadamard test is a fundamental subroutine in many quantum algorithms, including the Deutsch-Jozsa algorithm and quantum phase estimation [NC12]. In the first compensation circuit, $C(|+\rangle)$, Bob computes the Hadamard test while Alice performs a Pauli-Z gate conditioned on the Hadamard test's outcome. Specifically, Bob measures $|0\rangle$ with probability $p_r(0) = \frac{1+\mathrm{Re}\langle\psi|U|\psi\rangle}{2}$, and if he measures $|0\rangle$, Alice does not perform a Pauli-Z gate on her qubit. Conversely, if Bob measures $|1\rangle$, Alice performs the Z gate. Thus, Alice's execution of the Z gate is effectively conditioned on the real part of the expectation value of the teleported gate $\mathrm{Re}(\langle U\rangle)$. In the second compensation circuit, Alice's execution of the Z gate is conditioned on the imaginary part of the expectation value of the teleported gate $\mathrm{Im}(\langle U\rangle)$.

The error decomposition from Figure 3.7 presents challenges, such as the general nature of the operations Bob needs to implement. Additionally, the sampling overhead is unclear without a concrete implementation of these operations. However, when we restrict the gates we want to teleport to be hermitian, we can determine the sampling overhead. In Figures 3.8 and 3.9c, we present two practical error decompositions related to the work of Mitarai and Fujii [MF21]. The main observations include significant overlap in the circuits that comprise these decompositions. Furthermore, we improve the sampling overhead of the decomposition, which can be further enhanced by utilizing NME resource states in the gate teleportation circuit. We demonstrated this for controlled-{X, Y, Z, H} gates.

This thesis focuses primarily on augmenting circuit cutting with entanglement. However, an alternative perspective is to implement error mitigation within the teleportation protocol to address the absence of entanglement in the resource state. Quantum teleportation holds significant promise for the realization of a quantum internet [22; CCB18; CCC20]. Given the challenges associated with decoherence in entanglement creation, distribution, and storage, potentially leading to NME resource states, error mitigation strategies for quantum teleportation become relevant [BP07; CCT+20; KMSD19; LIK+21]. Therefore, a possible future application for our research is the implementation of gate teleportation within a quantum internet.

6 Related Work

In this chapter, we address related research focusing on circuit cutting. We begin by discussing the paper SSimulating Large Quantum Circuits on a Small Quantum Computer"by Peng et al. [PHOW20], which is foundational in the field of circuit cutting and has spurred much subsequent research. Peng et al. [PHOW20] introduced a cluster simulation scheme designed to simulate large quantum circuits on small quantum computers with limited quantum memory. Through the decomposition of the tensor network of a (K, d)-clustered quantum circuit, they illustrated how to simulate each cluster on a d-qubit machine. Their approach enables efficient simulation of quantum systems with weak interactions, particularly large molecules partitioned into smaller clusters. Furthermore, they applied their scheme to Variational Quantum Eigensolvers and experimentally demonstrated its efficacy in estimating the energy of the BeH_2 molecule using a physical quantum device with fewer qubits. Overall, their findings offer a systematic understanding of the trade-offs between classical and quantum computation, laying the groundwork for near-term quantum applications.

Wire cutting generally differs from gate cutting in that it involves splitting circuits at points along the wires, essentially breaking the connections between qubits rather than the gates themselves. However, wire cutting is closely related to our research. Therefore, we now address related research on wire cutting.

This thesis is greatly inspired by the research of Bechtold et al. [BBLM23; BBLM24], who presented a wire cutting technique based on quantum teleportation with NME states. They leverage NME states to reduce the wire cutting sampling overhead. By increasing the entanglement in resource states, they demonstrate a significant decrease in sampling overhead, underscoring the value of entanglement as a computational resource. The authors derive the optimal sampling overhead for arbitrary NME states and present a wire cut employing pure NME states that achieves this optimal overhead. Their method spans a range from optimal wire cuts without entanglement to quantum teleportation using maximally entangled states. These findings help bridge the gap between wire cutting and quantum teleportation using NME resource states, significantly improving the flexibility to implement distributed quantum computing.

Further advancements in wire cutting research were made by Lowe et al. [LMH+23] and Harada et al. [HWY23]. Lowe et al. [LMH+23] introduced a wire cutting method based on randomized measurements, demonstrating a quadratic runtime improvement over the current state of the art, particularly for circuits where multiple neighboring wires are simultaneously cut. Their approach necessitates classical communication between circuit fragments to coordinate measurement outcomes and state preparation. They demonstrated that for circuits structured with matrix product states, synchronization between circuit fragments can be achieved by iteratively executing smaller circuits, even on a single device. However, for general circuits, their algorithm requires multiple circuit executions across many devices, spatially separated rather than temporally. They also derived an information-theoretic lower bound, which is quadratically lower than their method. The authors

applied their method to the QAOA algorithm, highlighting practical and operational aspects for real devices, including algorithms based on randomized measure-and-prepare channels and sampling of the cut circuit. Their numerical simulations revealed significant speedups over previous state-of-the-art techniques for wire cutting. Furthermore, they conducted large-scale simulations of QAOA circuits over multiple GPUs, demonstrating that their software implementation of wire cutting methods, integrated with PennyLane, enables small-scale quantum devices to emulate the results of large circuits effectively. These results provide valuable insights into the practicality and scalability of circuit cutting workflows for quantum computation.

Harada et al. [HWY23] propose novel decompositions of identity channels within the framework of wire cutting to efficiently simulate large quantum circuits with limited resources. Their approach involves applying a grouping technique for mutually commuting observables to eliminate redundancy in measurement and state-preparation operations required for wire cutting. This results in a new decomposition of the parallel n-qubit identity channel, comprised of measurement-and-prepare channelss (MPCs) containing LOCC arising from the grouping. Notably, their method achieves lower bounds in both the sampling overhead and the number of MPCs, including an ancilla-free parallel wire cutting. Their decomposition significantly reduces the classical processing time for quantum circuit compilation and constructs quantum circuits efficiently with up to 12 qubits on fully connected qubit devices. Furthermore, their approach improves the worst-case sampling overhead for arbitrary n-wire cuts from $16k$ to $9k$ without requiring ancilla qubits. The authors also explore the application of mutually unbiased bases in their decomposition, highlighting potential connections to quantum state estimation. They discuss the extension of their optimal decomposition method to non-parallel wire cutting, acknowledging the challenge of achieving globally optimal cutting without additional ancilla qubits.

Next, we turn to research focused on gate cutting, similar to ours, some of which also leverage entanglement as a resource for distributed quantum computing. However, our research distinguishes itself from these studies by investigating the impact of NME resource states. Piveteau and Sutter [PS23] investigated the efficacy of classical communication in improving the efficiency of gate cutting techniques for simulating quantum circuits on devices with limited qubits. They divided the quantum circuit into two regions and utilized quasiprobability simulation to replace non-local gates with local operations in these regions. Their findings revealed that classical communication aids in reducing overhead for multiple instances of non-local gates, while offering no advantage for single instances of Clifford gates. Gate teleportation was used to simulate non-local gates with classical communication. These results hold significance for demonstrating quantum advantage and are relevant for near-term quantum computation with limited qubits.

Also closely related to our work is the research by Ufrecht et al. [UHS+24], who, like us, based their study on the gate teleportation circuit from Eisert et al. [EJPP00]. However, their focus was on cutting a two-qubit rotation gate. Ufrecht et al. [UHS+24] introduced a joint cutting technique for non-Clifford two-qubit rotation gates using virtual teleportation and proved its optimality. For parallel gates, they derived an ancilla-free optimal decomposition. They highlighted several key points: controlled rotation gates are equivalent to two-qubit rotation gates up to local unitary operations, and CNOT gates are special cases within this class. Their joint virtual teleportation protocol improves on previous methods by eliminating the need for classical communication and real-time feedback during quantum computation. This allows for sequential execution of cut circuits on the same hardware instead of parallel execution. Additionally, their alternative quasi-probability decomposition of pure-state density matrices achieves an exponential reduction in the number of

terms required, leading to an exponential reduction in the number of channels in the cutting scheme. Their method also enables ancilla-free optimal joint cutting schemes for CNOT gates, two-qubit rotation gates, and controlled rotation gates.

Akin to their aforementioned work, Ufrecht et al. [UPR+23] proposed a method for cutting multi-controlled Z (MCZ) gates using ZX-calculus and the H-box fusion rule. This approach decomposes MCZ gates into independent partitions, facilitating efficient evaluation of quantum circuits. They derived an upper bound on the sampling overhead regardless of the MCZ gate order. Validation on IBM hardware demonstrated significant noise reduction due to the reduced number of CNOT gates in the cut circuits. The method outperforms full circuit execution even under noisy conditions, highlighting its potential for practical quantum computing applications.

7 Conclusion

In this thesis, we explored the application of gate teleportation circuits for distributed quantum computing, focusing on the gate teleportation circuit from Eisert et al. [EJPP00] that implements non-local controlled two-qubit quantum gates via local operations using entanglement as a resource. We investigated the effects of employing NME resource states in this gate teleportation circuit, which introduces an error in the result. The magnitude of this error is directly related to the degree of entanglement in the resource state, with greater entanglement resulting in smaller errors and vice versa.

By decomposing the error, we demonstrated that a controlled quantum gate can be cut using gate teleportation with NME resource states, resulting in a sampling overhead between 1 and 3 depending on the degree of entanglement. This approach shows that gate cutting can leverage NME states to lower the sampling overhead compared to gate cutting without entanglement. We improved the compensation circuits by eliminating one ancilla qubit and thereby discovered a method for removing the ancilla qubit in various circuits alike. Furthermore, we identified two other decompositions of the compensation circuits closely related to the CZ decomposition from Mitarai and Fujii [MF21]. Both decompositions facilitate gate cuts without entanglement resources that improve the sampling overhead from 5 to 4 compared to the work of Mitarai and Fujii [MF21].

Our research bridges the gap between gate teleportation and gate cutting using NME resource states, similar to the findings of Bechtold et al. [BBLM23], who combined wire cutting and quantum teleportation using NME resource states. The significance of entanglement as a valuable computational resource in distributed quantum computing is highlighted by our results. By exploring the application of gate teleportation circuits with NME resource states, we have demonstrated a potential solution for reducing the sampling overhead in gate cutting, which could be crucial for the development of more efficient and reliable distributed quantum computing systems.

Future work may include refining the decompositions from Figures 3.7 and 3.9c to make them more general and efficient, as they currently do not work for arbitrary controlled gates and have a worse sampling overhead than the decomposition from Figure 3.6. Additionally, one may explore how the Hadamard test in Figure 3.6 can be replaced by direct measurements. Mitarai and Fujii [MF19] present such approach.

Bibliography

[22] *Quantum Communication, Quantum Networks, and Quantum Sensing*. Elsevier, 2022. ISBN: 9780128229422. DOI: 10.1016/C2019-0-05028-5 (cit. on pp. 13, 14, 38).

[AAB+19] F. Arute, K. Arya, R. Babbush, D. Bacon, J. C. Bardin, R. Barends, R. Biswas, S. Boixo, F. G. S. L. Brandao, D. A. Buell, B. Burkett, Y. Chen, Z. Chen, B. Chiaro, R. Collins, W. Courtney, A. Dunsworth, E. Farhi, B. Foxen, A. Fowler, C. Gidney, M. Giustina, R. Graff, K. Guerin, S. Habegger, M. P. Harrigan, M. J. Hartmann, A. Ho, M. Hoffmann, T. Huang, T. S. Humble, S. V. Isakov, E. Jeffrey, Z. Jiang, D. Kafri, K. Kechedzhi, J. Kelly, P. V. Klimov, S. Knysh, A. Korotkov, F. Kostritsa, D. Landhuis, M. Lindmark, E. Lucero, D. Lyakh, S. Mandrà, J. R. McClean, M. McEwen, A. Megrant, X. Mi, K. Michielsen, M. Mohseni, J. Mutus, O. Naaman, M. Neeley, C. Neill, M. Y. Niu, E. Ostby, A. Petukhov, J. C. Platt, C. Quintana, E. G. Rieffel, P. Roushan, N. C. Rubin, D. Sank, K. J. Satzinger, V. Smelyanskiy, K. J. Sung, M. D. Trevithick, A. Vainsencher, B. Villalonga, T. White, Z. J. Yao, P. Yeh, A. Zalcman, H. Neven, J. M. Martinis. "Quantum supremacy using a programmable superconducting processor". In: *Nature* 574.7779 (Oct. 2019), pp. 505–510. ISSN: 0028-0836. DOI: 10.1038/s41586-019-1666-5 (cit. on p. 11).

[AAS23] R. Abdelmagid, K. Alshehhi, G. Sadiek. "Entanglement Degradation in Two Interacting Qubits Coupled to Dephasing Environments". In: *Entropy* 25.10 (Oct. 2023), p. 1458. ISSN: 1099-4300. DOI: 10.3390/e25101458 (cit. on pp. 11, 14, 37).

[AP02] P. Agrawal, A. K. Pati. "Probabilistic quantum teleportation". In: *Physics Letters A* 305.1-2 (Nov. 2002), pp. 12–17. ISSN: 03759601. DOI: 10.1016/S0375-9601(02)01383-X (cit. on p. 15).

[Axl24] S. Axler. *Linear Algebra Done Right*. Cham: Springer International Publishing, 2024. ISBN: 978-3-031-41025-3. DOI: 10.1007/978-3-031-41026-0 (cit. on p. 29).

[BBC+93] C. H. Bennett, G. Brassard, C. Crépeau, R. Jozsa, A. Peres, W. K. Wootters. "Teleporting an unknown quantum state via dual classical and Einstein-Podolsky-Rosen channels". In: *Physical Review Letters* 70.13 (Mar. 1993), pp. 1895–1899. ISSN: 0031-9007. DOI: 10.1103/PhysRevLett.70.1895 (cit. on pp. 11, 15).

[BBLM23] M. Bechtold, J. Barzen, F. Leymann, A. Mandl. "Circuit Cutting with Non-Maximally Entangled States". In: (June 2023) (cit. on pp. 11, 14, 18, 37, 39, 43).

[BBLM24] M. Bechtold, J. Barzen, F. Leymann, A. Mandl. "Cutting a Wire with Non-Maximally Entangled States". In: (Feb. 2024) (cit. on pp. 11, 39).

[BP07] H.-P. Breuer, F. Petruccione. *The Theory of Open Quantum Systems*. Oxford University PressOxford, Jan. 2007. ISBN: 0199213909. DOI: 10.1093/acprof:oso/9780199213900.001.0001 (cit. on p. 38).

[BPK24] S. Brandhofer, I. Polian, K. Krsulich. "Optimal Partitioning of Quantum Circuits Using Gate Cuts and Wire Cuts". In: *IEEE Transactions on Quantum Engineering* 5 (2024), pp. 1–10. ISSN: 2689-1808. DOI: 10.1109/TQE.2023.3347106 (cit. on p. 18).

[BPS23] L. Brenner, C. Piveteau, D. Sutter. "Optimal wire cutting with classical communication". In: (Feb. 2023) (cit. on p. 18).

[CAF+22] M. Caleffi, M. Amoretti, D. Ferrari, D. Cuomo, J. Illiano, A. Manzalini, A. S. Cacciapuoti. "Distributed Quantum Computing: a Survey". In: (Dec. 2022) (cit. on p. 11).

[CCB18] M. Caleffi, A. S. Cacciapuoti, G. Bianchi. "Quantum internet". In: *Proceedings of the 5th ACM International Conference on Nanoscale Computing and Communication*. New York, NY, USA: ACM, Sept. 2018, pp. 1–4. ISBN: 9781450357111. DOI: 10.1145/3233188.3233224 (cit. on pp. 11, 38).

[CCC20] D. Cuomo, M. Caleffi, A. S. Cacciapuoti. "Towards a distributed quantum computing ecosystem". In: *IET Quantum Communication* 1.1 (2020). ISSN: 26328925. DOI: 10.1049/iet-qtc.2020.0002 (cit. on pp. 14, 38).

[CCT+20] A. S. Cacciapuoti, M. Caleffi, F. Tafuri, F. S. Cataliotti, S. Gherardini, G. Bianchi. "Quantum Internet: Networking Challenges in Distributed Quantum Computing". In: *IEEE Network* 34.1 (Jan. 2020), pp. 137–143. ISSN: 0890-8044. DOI: 10.1109/MNET.001.1900092 (cit. on pp. 14, 38).

[CCVH20] A. S. Cacciapuoti, M. Caleffi, R. Van Meter, L. Hanzo. "When Entanglement Meets Classical Communications: Quantum Teleportation for the Quantum Internet". In: *IEEE Transactions on Communications* 68.6 (June 2020), pp. 3808–3833. ISSN: 0090-6778. DOI: 10.1109/TCOMM.2020.2978071 (cit. on p. 14).

[CHL+23] D. T. Chen, E. H. Hansen, X. Li, V. Kulkarni, V. Chaudhary, B. Ren, Q. Guan, S. Kuppannagari, J. Liu, S. Xu. "Efficient Quantum Circuit Cutting by Neglecting Basis Elements". In: (Apr. 2023) (cit. on p. 17).

[CTV17] E. T. Campbell, B. M. Terhal, C. Vuillot. "Roads towards fault-tolerant universal quantum computation". In: *Nature* 549.7671 (Sept. 2017), pp. 172–179. ISSN: 0028-0836. DOI: 10.1038/nature23460 (cit. on pp. 11, 37).

[Cuo23] D. Cuomo. "Architectures and circuits for distributed quantum computing". In: (July 2023) (cit. on p. 11).

[CY13] S. M. Cohen, L. Yu. "All unitaries having operator Schmidt rank 2 are controlled unitaries". In: *Physical Review A* 87.2 (Feb. 2013), p. 022329. ISSN: 1050-2947. DOI: 10.1103/PhysRevA.87.022329 (cit. on p. 17).

[DK17] A. Daskin, S. Kais. "An ancilla-based quantum simulation framework for non-unitary matrices". In: *Quantum Information Processing* 16.1 (Jan. 2017), p. 33. ISSN: 1570-0755. DOI: 10.1007/s11128-016-1452-3 (cit. on p. 29).

[DWLJ23] Y. Ding, Y. Wei, Z. Li, M. Jiang. "Quantum teleportation based on non-maximally entangled graph states". In: *Quantum Information Processing* 22.11 (Nov. 2023), p. 400. ISSN: 1573-1332. DOI: 10.1007/s11128-023-04157-0 (cit. on p. 14).

[EJPP00] J. Eisert, K. Jacobs, P. Papadopoulos, M. B. Plenio. "Optimal local implementation of nonlocal quantum gates". In: *Physical Review A* 62.5 (Oct. 2000), p. 052317. ISSN: 1050-2947. DOI: 10.1103/PhysRevA.62.052317 (cit. on pp. 12, 16, 21, 22, 24, 32, 37, 40, 43).

[FYKI12] K. Fujii, T. Yamamoto, M. Koashi, N. Imoto. "A distributed architecture for scalable quantum computation with realistically noisy devices". In: (Feb. 2012) (cit. on p. 11).

[GCS17] J. M. Gambetta, J. M. Chow, M. Steffen. "Building logical qubits in a superconducting quantum computing system". In: *npj Quantum Information* 3.1 (Jan. 2017), p. 2. ISSN: 2056-6387. DOI: 10.1038/s41534-016-0004-0 (cit. on p. 11).

[GPAY23] A. M. Gomez, T. L. Patti, A. Anandkumar, S. F. Yelin. "Near-Term Distributed Quantum Computation using Mean-Field Corrections and Auxiliary Qubits". In: (Sept. 2023) (cit. on pp. 11, 37).

[Gro96] L. K. Grover. "A fast quantum mechanical algorithm for database search". In: *Proceedings of the twenty-eighth annual ACM symposium on Theory of computing - STOC '96*. New York, New York, USA: ACM Press, 1996, pp. 212–219. ISBN: 0897917855. DOI: 10.1145/237814.237866 (cit. on p. 11).

[GTC22] G. González-García, R. Trivedi, J. I. Cirac. "Error Propagation in NISQ Devices for Solving Classical Optimization Problems". In: *PRX Quantum* 3.4 (Dec. 2022), p. 040326. ISSN: 2691-3399. DOI: 10.1103/PRXQuantum.3.040326 (cit. on p. 14).

[Hil24] M. Hildebrand. *GitHub - Investigating Gate Teleportation with NME states for Gate Cutting*. June 2024. URL: https://github.com/infacc/nme-gt (cit. on pp. 21, 51).

[HJ85] R. A. Horn, C. R. Johnson. *Matrix Analysis*. Cambridge University Press, Dec. 1985. ISBN: 9780521386326. DOI: 10.1017/CBO9780511810817 (cit. on p. 29).

[HM17] A. W. Harrow, A. Montanaro. "Quantum computational supremacy". In: *Nature* 549.7671 (Sept. 2017), pp. 203–209. ISSN: 0028-0836. DOI: 10.1038/nature23458 (cit. on p. 11).

[HWY23] H. Harada, K. Wada, N. Yamamoto. "Doubly optimal parallel wire cutting without ancilla qubits". In: (Mar. 2023) (cit. on pp. 39, 40).

[JTK+24] A. Javadi-Abhari, M. Treinish, K. Krsulich, C. J. Wood, J. Lishman, J. Gacon, S. Martiel, P. D. Nation, L. S. Bishop, A. W. Cross, B. R. Johnson, J. M. Gambetta. "Quantum computing with Qiskit". In: (May 2024) (cit. on p. 35).

[KBF+15] J. Kelly, R. Barends, A. G. Fowler, A. Megrant, E. Jeffrey, T. C. White, D. Sank, J. Y. Mutus, B. Campbell, Y. Chen, Z. Chen, B. Chiaro, A. Dunsworth, I.-C. Hoi, C. Neill, P. J. J. O'Malley, C. Quintana, P. Roushan, A. Vainsencher, J. Wenner, A. N. Cleland, J. M. Martinis. "State preservation by repetitive error detection in a superconducting quantum circuit". In: *Nature* 519.7541 (Mar. 2015), pp. 66–69. ISSN: 0028-0836. DOI: 10.1038/nature14270 (cit. on p. 11).

[KMSD19] S. Khatri, C. T. Matyas, A. U. Siddiqui, J. P. Dowling. "Practical figures of merit and thresholds for entanglement distribution in quantum networks". In: *Physical Review Research* 1.2 (Sept. 2019), p. 023032. ISSN: 2643-1564. DOI: 10.1103/PhysRevResearch.1.023032 (cit. on pp. 11, 37, 38).

[LIK+21] N. P. de Leon, K. M. Itoh, D. Kim, K. K. Mehta, T. E. Northup, H. Paik, B. S. Palmer, N. Samarth, S. Sangtawesin, D. W. Steuerman. "Materials challenges and opportunities for quantum computing hardware". In: *Science* 372.6539 (Apr. 2021). ISSN: 0036-8075. DOI: 10.1126/science.abb2823 (cit. on p. 38).

[LMH+23] A. Lowe, M. Medvidović, A. Hayes, L. J. O'Riordan, T. R. Bromley, J. M. Arrazola, N. Killoran. "Fast quantum circuit cutting with randomized measurements". In: *Quantum* 7 (2023). ISSN: 2521327X. DOI: 10.22331/Q-2023-03-02-934 (cit. on p. 39).

[MF19] K. Mitarai, K. Fujii. "Methodology for replacing indirect measurements with direct measurements". In: *Physical Review Research* 1.1 (Aug. 2019), p. 013006. ISSN: 2643-1564. DOI: 10.1103/PhysRevResearch.1.013006 (cit. on p. 43).

[MF21] K. Mitarai, K. Fujii. "Constructing a virtual two-qubit gate by sampling single-qubit operations". In: *New Journal of Physics* 23.2 (2021). ISSN: 13672630. DOI: 10.1088/1367-2630/abd7bc (cit. on pp. 18, 21, 31, 32, 38, 43).

[MK13] C. Monroe, J. Kim. "Scaling the Ion Trap Quantum Processor". In: *Science* 339.6124 (Mar. 2013), pp. 1164–1169. ISSN: 0036-8075. DOI: 10.1126/science.1231298 (cit. on pp. 11, 37).

[MN18] A. Müller-Hermes, I. Nechita. "Operator Schmidt ranks of bipartite unitary matrices". In: *Linear Algebra and its Applications* 557 (Nov. 2018), pp. 174–187. ISSN: 00243795. DOI: 10.1016/j.laa.2018.07.018 (cit. on pp. 16, 17).

[NC12] M. A. Nielsen, I. L. Chuang. *Quantum Computation and Quantum Information*. Cambridge University Press, June 2012. ISBN: 9781107002173. DOI: 10.1017/CBO9780511976667 (cit. on pp. 14, 19, 38).

[PHOW20] T. Peng, A. W. Harrow, M. Ozols, X. Wu. "Simulating Large Quantum Circuits on a Small Quantum Computer". In: *Physical Review Letters* 125.15 (2020). ISSN: 10797114. DOI: 10.1103/PhysRevLett.125.150504 (cit. on pp. 11, 39).

[PP19] K. G. Paulson, P. K. Panigrahi. "Tripartite non-maximally-entangled mixed states as a resource for optimally controlled quantum teleportation fidelity". In: *Physical Review A* 100.5 (Nov. 2019), p. 052325. ISSN: 2469-9926. DOI: 10.1103/PhysRevA.100.052325 (cit. on p. 14).

[Pre18] J. Preskill. "Quantum Computing in the NISQ era and beyond". In: (Jan. 2018). DOI: 10.22331/q-2018-08-06-79 (cit. on pp. 11, 37).

[PS23] C. Piveteau, D. Sutter. "Circuit knitting with classical communication". In: *IEEE Transactions on Information Theory* (2023). ISSN: 15579654. DOI: 10.1109/TIT.2023.3310797 (cit. on pp. 11, 40).

[PSSO21] M. A. Perlin, Z. H. Saleem, M. Suchara, J. C. Osborn. "Quantum circuit cutting with maximum-likelihood tomography". In: *npj Quantum Information* 7.1 (Apr. 2021), p. 64. ISSN: 2056-6387. DOI: 10.1038/s41534-021-00390-6 (cit. on p. 17).

[PV12] H. Prakash, V. Verma. "Minimum assured fidelity and minimum average fidelity in quantum teleportation of single qubit using non-maximally entangled states". In: *Quantum Information Processing* 11.6 (Dec. 2012), pp. 1951–1959. ISSN: 1570-0755. DOI: 10.1007/s11128-011-0348-5 (cit. on p. 14).

[SG11] D. Stahlke, R. B. Griffiths. “Entanglement requirements for implementing bipartite unitary operations”. In: *Physical Review A* 84.3 (Sept. 2011), p. 032316. ISSN: 1050-2947. DOI: 10.1103/PhysRevA.84.032316 (cit. on p. 16).

[Sho] P. Shor. “Algorithms for quantum computation: discrete logarithms and factoring”. In: *Proceedings 35th Annual Symposium on Foundations of Computer Science*. IEEE Comput. Soc. Press, pp. 124–134. ISBN: 0-8186-6580-7. DOI: 10.1109/SFCS.1994.365700 (cit. on p. 11).

[SHS+22] A. W. Schlimgen, K. Head-Marsden, L. M. Sager-Smith, P. Narang, D. A. Mazziotti. “Quantum state preparation and nonunitary evolution with diagonal operators”. In: *Physical Review A* 106.2 (Aug. 2022), p. 022414. ISSN: 2469-9926. DOI: 10.1103/PhysRevA.106.022414 (cit. on p. 29).

[SPS23] L. Schmitt, C. Piveteau, D. Sutter. “Cutting circuits with multiple two-qubit unitaries”. In: (Dec. 2023) (cit. on p. 18).

[SZ21] M. Sarvaghad-Moghaddam, M. Zomorodi. “A general protocol for distributed quantum gates”. In: *Quantum Information Processing* 20.8 (Aug. 2021), p. 265. ISSN: 1570-0755. DOI: 10.1007/s11128-021-03191-0 (cit. on p. 37).

[TCC+22] J. Tilly, H. Chen, S. Cao, D. Picozzi, K. Setia, Y. Li, E. Grant, L. Wossnig, I. Rungger, G. H. Booth, J. Tennyson. “The Variational Quantum Eigensolver: A review of methods and best practices”. In: *Physics Reports* 986 (Nov. 2022), pp. 1–128. ISSN: 03701573. DOI: 10.1016/j.physrep.2022.08.003 (cit. on p. 19).

[TTS+21] W. Tang, T. Tomesh, M. Suchara, J. Larson, M. Martonosi. “CutQC: using small Quantum computers for large Quantum circuit evaluations”. In: *Proceedings of the 26th ACM International Conference on Architectural Support for Programming Languages and Operating Systems*. New York, NY, USA: ACM, Apr. 2021, pp. 473–486. ISBN: 9781450383172. DOI: 10.1145/3445814.3446758 (cit. on p. 17).

[UHS+24] C. Ufrecht, L. S. Herzog, D. D. Scherer, M. Periyasamy, S. Rietsch, A. Plinge, C. Mutschler. “Optimal joint cutting of two-qubit rotation gates”. In: *Physical Review A* 109.5 (May 2024), p. 052440. ISSN: 2469-9926. DOI: 10.1103/PhysRevA.109.052440 (cit. on p. 40).

[UPR+23] C. Ufrecht, M. Periyasamy, S. Rietsch, D. D. Scherer, A. Plinge, C. Mutschler. “Cutting multi-control quantum gates with ZX calculus”. In: *Quantum* 7 (Oct. 2023), p. 1147. ISSN: 2521-327X. DOI: 10.22331/q-2023-10-23-1147 (cit. on pp. 18, 41).

[WJEK99] A. G. White, D. F. V. James, P. H. Eberhard, P. G. Kwiat. “Nonmaximally Entangled States: Production, Characterization, and Utilization”. In: *Physical Review Letters* 83.16 (Oct. 1999), pp. 3103–3107. ISSN: 0031-9007. DOI: 10.1103/PhysRevLett.83.3103 (cit. on p. 14).

[WTYK15] X.-W. Wang, S.-Q. Tang, J.-B. Yuan, L.-M. Kuang. “Nonmaximally Entangled States can be Better for Quantum Correlation Distribution and Storage”. In: *International Journal of Theoretical Physics* 54.5 (May 2015), pp. 1461–1469. ISSN: 0020-7748. DOI: 10.1007/s10773-014-2343-y (cit. on p. 14).

[YY10] F. Yan, T. Yan. “Probabilistic teleportation via a non-maximally entangled GHZ state”. In: *Chinese Science Bulletin* 55.10 (Apr. 2010), pp. 902–906. ISSN: 1001-6538. DOI: 10.1007/s11434-009-0725-y (cit. on p. 15).

All links were last followed on June 4, 2024.

A Calculations

This appendix contains the calculations that were too extensive to be included in the main text of this thesis. We use the notation and variables defined in Chapter 3 throughout this appendix. This includes $|\tau_{|\phi_{1,2}\rangle}\rangle$, $|\psi\rangle$, ρ, $\rho_{|\phi_{1,2}\rangle}$ (Equations (3.1) to (3.4)), E_ρ (Equation (3.18)), $|\tau'_G\rangle$ (Equation (3.28)), and ρ'_G (Equation (3.29)).

Since we analyze a four-qubit gate teleportation circuit and focus on its reduced two-qubit result, many calculations involve complex 4×4 matrices with entries derived from multiple variables, which cannot always be expressed compactly in tensor products. Therefore, we provide a Jupyter Notebook with these calculations [Hil24]. In this Jupyter Notebook, the calculations are implemented using SymPy. For a more detailed understanding of these calculations, refer to the notebook.

A.1 Controlled Gate Decomposition

In this section, we provide calculations for the decomposition shown in Figure 2.4. For convinience, we label the 10 subcircuits $s_0^U, \ldots, s_9^U$ for $U \in \{X, Y, Z, H\}$ as shown in Equation (A.1).

$$CU = \frac{1}{2}\Bigg[\underbrace{\begin{matrix} e^{i\pi Z/4} \\ e^{i\pi U/4} \end{matrix}}_{s_0^U} + \underbrace{\begin{matrix} e^{-i\pi Z/4} \\ e^{-i\pi U/4} \end{matrix}}_{s_1^U} - \underbrace{\begin{matrix} \frac{I-Z}{2} \\ \text{———} \end{matrix}}_{s_2^U} - \underbrace{\begin{matrix} \text{———} \\ \frac{I-U}{2} \end{matrix}}_{s_3^U} + \underbrace{\begin{matrix} \text{———} \\ e^{i\pi U/2} \end{matrix}}_{s_4^U} \Bigg. \tag{A.1}$$
$$\Bigg. + \underbrace{\begin{matrix} \text{———} \\ \frac{I+U}{2} \end{matrix}}_{s_5^U} + \underbrace{\begin{matrix} \frac{I+Z}{2} \\ \text{———} \end{matrix}}_{s_6^U} + \underbrace{\begin{matrix} e^{i\pi Z/2} \\ \frac{I-U}{2} \end{matrix}}_{s_7^U} - \underbrace{\begin{matrix} \frac{I+Z}{2} \\ e^{i\pi U/2} \end{matrix}}_{s_8^U} - \underbrace{\begin{matrix} e^{i\pi Z/2} \\ \frac{I+Z}{2} \end{matrix}}_{s_9^U} \Bigg]$$

Furthermore, we denote by $s_i(\rho)$ for $i \in \{0, \ldots, 9\}$ the density matrix of the mixed state ρ after applying the circuit s_i, as defined in Equation (A.2).

$$s_i^U(\rho) := s_i^U \cdot \rho \cdot \left(s_i^U\right)^\dagger \tag{A.2}$$

Since writing down the individual $s_i^U(\rho)$ matrices would be very confusing and would have little added value, we limit ourselves here to the summed result matrices in Equations (A.3) to (A.10) corresponding to the decomposition. For more details, please refer to [**infacc2024GitHubCutting**].

$$(CX)\rho(CX)^\dagger = \begin{bmatrix} a\overline{a} & a\overline{b} & a\overline{d} & a\overline{c} \\ b\overline{a} & b\overline{b} & b\overline{d} & b\overline{c} \\ d\overline{a} & d\overline{b} & d\overline{d} & d\overline{c} \\ c\overline{a} & c\overline{b} & c\overline{d} & c\overline{c} \end{bmatrix} \tag{A.3}$$

$$= \frac{1}{2}\left(\sum_{i\in 0,1,4,5,6,7} s_i^X(\rho) - \sum_{i\in\{2,3,8,9\}} s_i^X(\rho) \right) \tag{A.4}$$

$$(CY)\rho(CY)^\dagger = \begin{bmatrix} a\overline{a} & a\overline{b} & ia\overline{d} & -ia\overline{c} \\ b\overline{a} & b\overline{b} & ib\overline{d} & -ib\overline{c} \\ -id\overline{a} & -id\overline{b} & d\overline{d} & -d\overline{c} \\ ic\overline{a} & ic\overline{b} & -c\overline{d} & c\overline{c} \end{bmatrix} \tag{A.5}$$

$$= \frac{1}{2}\left(\sum_{i\in 0,1,4,5,6,7} s_i^Y(\rho) - \sum_{i\in\{2,3,8,9\}} s_i^Y(\rho) \right) \tag{A.6}$$

$$(CZ)\rho(CZ)^\dagger = \begin{bmatrix} a\overline{a} & a\overline{b} & a\overline{c} & -a\overline{d} \\ b\overline{a} & b\overline{b} & b\overline{c} & -b\overline{d} \\ c\overline{a} & c\overline{b} & c\overline{c} & -c\overline{d} \\ -d\overline{a} & -d\overline{b} & -d\overline{c} & d\overline{d} \end{bmatrix} \tag{A.7}$$

$$= \frac{1}{2}\left(\sum_{i\in 0,1,4,5,6,7} s_i^Z(\rho) - \sum_{i\in\{2,3,8,9\}} s_i^Z(\rho) \right) \tag{A.8}$$

$$(CH)\rho(CH)^\dagger = \begin{bmatrix} a\overline{a} & a\overline{b} & \frac{\sqrt{2}a\left(\overline{c}+\overline{d}\right)}{2} & \frac{\sqrt{2}a\left(\overline{c}-\overline{d}\right)}{2} \\ b\overline{a} & b\overline{b} & \frac{\sqrt{2}b\left(\overline{c}+\overline{d}\right)}{2} & \frac{\sqrt{2}b\left(\overline{c}-\overline{d}\right)}{2} \\ \frac{\sqrt{2}(c+d)\overline{a}}{2} & \frac{\sqrt{2}(c+d)\overline{b}}{2} & \frac{(c+d)\left(\overline{c}+\overline{d}\right)}{2} & \frac{(c+d)\left(\overline{c}-\overline{d}\right)}{2} \\ \frac{\sqrt{2}(c-d)\overline{a}}{2} & \frac{\sqrt{2}(c-d)\overline{b}}{2} & \frac{(c-d)\left(\overline{c}+\overline{d}\right)}{2} & \frac{(-c+d)\overline{d}}{2} + \frac{(c-d)\overline{c}}{2} \end{bmatrix} \tag{A.9}$$

$$= \frac{1}{2}\left(\sum_{i\in 0,1,4,5,6,7} s_i^H(\rho) - \sum_{i\in\{2,3,8,9\}} s_i^H(\rho) \right) \tag{A.10}$$

A.2 Hadamard Test

The Hadamard tests used to estimate the real ($|\Psi_r\rangle$) and imaginary ($|\Psi_i\rangle$) components of $\langle\psi| U |\psi\rangle$ yield the following states, respectively. The states are calculated in Equations (A.11) to (A.18)

$$|\Psi_r\rangle = (H \otimes I)(CU) |+\rangle |\psi\rangle \tag{A.11}$$
$$= (H \otimes I)\frac{1}{\sqrt{2}}(|0\rangle |\psi\rangle + |1\rangle U |\psi\rangle) \tag{A.12}$$
$$= \frac{1}{2}(|0\rangle (|\psi\rangle + U |\psi\rangle) + |1\rangle (|\psi\rangle - U |\psi\rangle)) \tag{A.13}$$
$$= |0\rangle \frac{I+U}{2} |\psi\rangle + |1\rangle \frac{I-U}{2} |\psi\rangle \tag{A.14}$$

$$|\Psi_i\rangle = (H \otimes I)(CU) |-i\rangle |\psi\rangle \tag{A.15}$$
$$= (H \otimes I)\frac{1}{\sqrt{2}}(|0\rangle |\psi\rangle - i |1\rangle U |\psi\rangle) \tag{A.16}$$
$$= \frac{1}{2}(|0\rangle (|\psi\rangle - iU |\psi\rangle) + |1\rangle (|\psi\rangle + iU |\psi\rangle)) \tag{A.17}$$
$$= |0\rangle \frac{I-iU}{2} |\psi\rangle + |1\rangle \frac{I+iU}{2} |\psi\rangle \tag{A.18}$$

Following that, we compute the probabilities of measuring the ancilla qubit in the state $|0\rangle$. We designate $p_r(x)$, where $x \in \{0, 1\}$, as the probability of measuring $|x\rangle$ on $|\Psi_r\rangle$. Similarly, we designate $p_i(x)$, where $x \in \{0, 1\}$, as the probability of measuring $|x\rangle$ on $|\Psi_i\rangle$. See Equations (A.19) to (A.36).

$$p_r(0) = \left|(|0\rangle \langle 0| \otimes I)\left(|0\rangle \frac{I+U}{2} |\psi\rangle + |1\rangle \frac{I-U}{2} |\psi\rangle\right)\right|^2 \tag{A.19}$$
$$= \left||0\rangle \frac{I+U}{2} |\psi\rangle\right|^2 \tag{A.20}$$
$$= ||0\rangle|^2 \left|\frac{I+U}{2} |\psi\rangle\right|^2 \tag{A.21}$$
$$= \langle\psi| \frac{I+U^\dagger}{2}\frac{I+U}{2} |\psi\rangle \tag{A.22}$$
$$= \frac{\langle\psi| (I + U + U^\dagger + U^\dagger U) |\psi\rangle}{4} \tag{A.23}$$
$$= \frac{\langle\psi| 2I |\psi\rangle + \langle\psi| U |\psi\rangle + \langle\psi| U^\dagger |\psi\rangle}{4} \tag{A.24}$$
$$= \frac{2 + \langle\psi| U |\psi\rangle + \langle\psi| U^\dagger |\psi\rangle}{4} \tag{A.25}$$
$$= \frac{2 + \langle\psi| (U + U^\dagger) |\psi\rangle}{4} \qquad z \in \mathbb{C} : \mathrm{Re}(z) = \frac{z + \overline{z}}{2} \tag{A.26}$$
$$= \frac{1 + \mathrm{Re}\,\langle\psi| U |\psi\rangle}{2} \tag{A.27}$$

$$p_i(0) = \left| (|0\rangle \langle 0| \otimes I) \left(|0\rangle \frac{I - iU}{2} |\psi\rangle + |1\rangle \frac{I + iU}{2} |\psi\rangle \right) \right|^2 \tag{A.28}$$

$$= \left| |0\rangle \frac{I - iU}{2} |\psi\rangle \right|^2 \tag{A.29}$$

$$= |\,|0\rangle\,|^2 \left| \frac{I - iU}{2} |\psi\rangle \right|^2 \tag{A.30}$$

$$= \langle\psi| \frac{I + iU^\dagger}{2} \frac{I - iU}{2} |\psi\rangle \tag{A.31}$$

$$= \frac{\langle\psi| (I - iU + iU^\dagger + U^\dagger U) |\psi\rangle}{4} \tag{A.32}$$

$$= \frac{\langle\psi| 2I |\psi\rangle - \langle\psi| iU |\psi\rangle + \langle\psi| iU^\dagger |\psi\rangle}{4} \tag{A.33}$$

$$= \frac{2 - i \langle\psi| U |\psi\rangle + i \langle\psi| U^\dagger |\psi\rangle}{4} \tag{A.34}$$

$$= \frac{2 + i \langle\psi| (U^\dagger - U) |\psi\rangle}{4} \qquad z \in \mathbb{C} : \mathrm{Im}(z) = \frac{z - \overline{z}}{2i} \tag{A.35}$$

$$= \frac{1 + \mathrm{Im} \langle\psi| U |\psi\rangle}{2} \tag{A.36}$$

For completeness, in Equations (A.37) to (A.42) we compute the probabilities of measuring the state $|1\rangle$ in the ancilla qubit for the states $|\Psi_r\rangle$ and $|\Psi_i\rangle$.

$$p_r(1) = 1 - p_r(0) \tag{A.37}$$

$$= 1 - \frac{1 + \mathrm{Re} \langle\psi| U |\psi\rangle}{2} \tag{A.38}$$

$$= \frac{1 - \mathrm{Re} \langle\psi| U |\psi\rangle}{2} \tag{A.39}$$

$$p_i(1) = 1 - p_i(0) \tag{A.40}$$

$$= 1 - \frac{1 + \mathrm{Im} \langle\psi| U |\psi\rangle}{2} \tag{A.41}$$

$$= \frac{1 - \mathrm{Im} \langle\psi| U |\psi\rangle}{2} \tag{A.42}$$

A.3 Equivalence of Compensation Circuits

In this section, we show the equivalences of Equations (3.19), (3.21) and (3.22). To prove the equivalence of Equation (3.21), we compute the respective final states before measurements in Equations (A.43) to (A.56) and compare them.

$$|\tau_{|++\rangle}\rangle = CZ_{1,2}H_1CU_{1,3}CX_{0,1}CX_{2,0}\left(|++\rangle|\psi\rangle\right) \tag{A.43}$$
$$= CZ_{1,2}H_1CU_{1,3}CX_{0,1}\left(|++\rangle|\psi\rangle\right) \tag{A.44}$$
$$= CZ_{1,2}H_1CU_{1,3}\left(|++\rangle|\psi\rangle\right) \tag{A.45}$$
$$= CZ_{1,2}H_1\left(\frac{|+0\rangle|\psi\rangle + |+1\rangle \otimes ((I\otimes U)|\psi\rangle)}{\sqrt{2}}\right) \tag{A.46}$$
$$= CZ_{1,2}\left(\frac{|++\rangle|\psi\rangle + |+-\rangle \otimes ((I\otimes U)|\psi\rangle)}{\sqrt{2}}\right) \tag{A.47}$$
$$= \frac{1}{2}(|+0\rangle|\psi\rangle + |+1\rangle \otimes ((Z\otimes I)|\psi\rangle) + |+0\rangle \otimes ((I\otimes U)|\psi\rangle) - |+1\rangle \otimes ((Z\otimes U)|\psi\rangle)) \tag{A.48}$$
$$= \frac{1}{2}\left(|+0\rangle \otimes ((I\otimes (I+U))|\psi\rangle) + |+1\rangle \otimes ((Z\otimes (I-U))|\psi\rangle)\right) \tag{A.49}$$

$$|\tau_{|--\rangle}\rangle = CZ_{1,2}H_1CU_{1,3}CX_{0,1}CX_{2,0}\left(|--\rangle|\psi\rangle\right) \tag{A.50}$$
$$= CZ_{1,2}H_1CU_{1,3}CX_{0,1}\left(|--\rangle \otimes ((Z\otimes I)|\psi\rangle)\right) \tag{A.51}$$
$$= CZ_{1,2}H_1CU_{1,3}\left(|+-\rangle \otimes ((Z\otimes I)|\psi\rangle)\right) \tag{A.52}$$
$$= CZ_{1,2}H_1\left(\frac{|+0\rangle \otimes ((Z\otimes I)|\psi\rangle) - |+1\rangle \otimes ((Z\otimes U)|\psi\rangle)}{\sqrt{2}}\right) \tag{A.53}$$
$$= CZ_{1,2}\left(\frac{|++\rangle \otimes ((Z\otimes I)|\psi\rangle) - |+-\rangle \otimes ((Z\otimes U)|\psi\rangle)}{\sqrt{2}}\right) \tag{A.54}$$
$$= \frac{1}{2}(|+0\rangle \otimes ((Z\otimes I)|\psi\rangle) + |+1\rangle|\psi\rangle - |+0\rangle \otimes ((Z\otimes U)|\psi\rangle) + |+1\rangle \otimes ((I\otimes U)|\psi\rangle)) \tag{A.55}$$
$$= \frac{1}{2}\left(|+0\rangle \otimes ((Z\otimes (I-U))|\psi\rangle) + |+1\rangle \otimes ((I\otimes (I+U))|\psi\rangle)\right) \tag{A.56}$$

When we compare Equation (A.49) and Equation (A.56), we can see that after measuring the qubits that initially hold the resource state, Bob and Alice's state collapses in one of the two states $\left(I\otimes\frac{I+U}{2}\right)|\psi\rangle$ or $\left(Z\otimes\frac{I-U}{2}\right)|\psi\rangle$ with equal probability. The corresponding density matrices are therefore equal in accordance to Equation (A.57).

$$\rho_{|++\rangle} = \left(I\otimes\frac{I+U}{2}\right)\rho\left(I\otimes\frac{I+U}{2}\right)^\dagger + \left(Z\otimes\frac{I-U}{2}\right)\rho\left(Z\otimes\frac{I-U}{2}\right)^\dagger = \rho_{|--\rangle} \tag{A.57}$$

Next, we show the same for the equivalence of Equation (3.22). We start by calculationg $|\tau_{|ii\rangle}\rangle$ and $|\tau_{|-i-i\rangle}\rangle$ in Equations (A.58) to (A.70).

$$|\tau_{|ii\rangle}\rangle = CZ_{1,2}H_1CU_{1,3}CX_{0,1}CX_{2,0}\left(|ii\rangle|\psi\rangle\right) \tag{A.58}$$

$$= CZ_{1,2}H_1CU_{1,3}CX_{0,1}\left(|ii\rangle \otimes (a|00\rangle + b|01\rangle) + i|{-ii}\rangle \otimes (c|10\rangle + d|11\rangle)\right) \tag{A.59}$$

$$= CZ_{1,2}H_1CU_{1,3}\left(\frac{|0i\rangle \otimes ((S\otimes I)|\psi\rangle) - |1{-}i\rangle \otimes ((S^\dagger \otimes I)|\psi\rangle)}{\sqrt{2}}\right) \tag{A.60}$$

$$= CZ_{1,2}H_1\Bigg(\frac{|00\rangle \otimes ((S\otimes I)|\psi\rangle) - |10\rangle \otimes ((S^\dagger \otimes I)|\psi\rangle)}{2} + \frac{|01\rangle \otimes ((S\otimes iU)|\psi\rangle) + |11\rangle \otimes ((S^\dagger \otimes iU)|\psi\rangle)}{2}\Bigg) \tag{A.61}$$

$$= CZ_{1,2}\Bigg(\frac{|0+\rangle \otimes ((S\otimes I)|\psi\rangle) - |1+\rangle \otimes ((S^\dagger \otimes I)|\psi\rangle)}{2} + \frac{|0-\rangle \otimes ((S\otimes iU)|\psi\rangle) + |1-\rangle \otimes ((S^\dagger \otimes iU)|\psi\rangle)}{2}\Bigg) \tag{A.62}$$

$$= CZ_{1,2}\Bigg(\frac{|00\rangle \otimes ((S\otimes \frac{I+iU}{2})|\psi\rangle) - |01\rangle \otimes ((S\otimes \frac{I-iU}{2})|\psi\rangle)}{\sqrt{2}} - \frac{|10\rangle \otimes ((S^\dagger \otimes \frac{I-iU}{2})|\psi\rangle) + |11\rangle \otimes ((S^\dagger \otimes \frac{I+iU}{2})|\psi\rangle)}{\sqrt{2}}\Bigg) \tag{A.63}$$

$$= \frac{1}{\sqrt{2}}\left(|\Phi^-\rangle \otimes \left(\left(S\otimes\frac{I+iU}{2}\right)|\psi\rangle\right) + |\Psi^-\rangle \otimes \left(\left(S^\dagger\otimes\frac{I-iU}{2}\right)|\psi\rangle\right)\right) \tag{A.64}$$

$$|\tau_{|-i-i\rangle}\rangle = CZ_{1,2}H_1CU_{1,3}CX_{0,1}CX_{2,0}\left(|{-i}{-i}\rangle|\psi\rangle\right) \tag{A.65}$$

$$= CZ_{1,2}H_1CU_{1,3}CX_{0,1}\left(|{-i}{-i}\rangle \otimes (a|00\rangle + b|01\rangle) - i|i{-i}\rangle \otimes (c|10\rangle + d|11\rangle)\right) \tag{A.66}$$

$$= CZ_{1,2}H_1CU_{1,3}\left(\frac{|0{-}i\rangle \otimes ((S^\dagger\otimes I)|\psi\rangle) - |1i\rangle \otimes ((S\otimes I)|\psi\rangle)}{\sqrt{2}}\right) \tag{A.67}$$

$$= CZ_{1,2}H_1\Bigg(\frac{|00\rangle \otimes ((S^\dagger \otimes I)|\psi\rangle) - |10\rangle \otimes ((S\otimes I)|\psi\rangle)}{2} - \frac{|01\rangle \otimes ((S^\dagger \otimes iU)|\psi\rangle) - |11\rangle \otimes ((S\otimes iU)|\psi\rangle)}{2}\Bigg) \tag{A.68}$$

$$= CZ_{1,2}\Bigg(\frac{|00\rangle \otimes ((S^\dagger \otimes \frac{I-iU}{2})|\psi\rangle) - |01\rangle \otimes ((S^\dagger \otimes \frac{I+iU}{2}))|\psi\rangle}{\sqrt{2}} - \frac{|10\rangle \otimes ((S\otimes \frac{I+iU}{2})|\psi\rangle) + |11\rangle \otimes ((S\otimes \frac{I-iU}{2})|\psi\rangle)}{\sqrt{2}}\Bigg) \tag{A.69}$$

$$= \frac{1}{\sqrt{2}}\left(|\Phi^-\rangle \otimes \left(\left(S^\dagger\otimes\frac{I-iU}{2}\right)|\psi\rangle\right) + |\Psi^-\rangle \otimes \left(\left(S\otimes\frac{I+iU}{2}\right)|\psi\rangle\right)\right) \tag{A.70}$$

Equations (A.64) and (A.70) show that, after measuring qubits 1 and 2, $|\tau_{|ii\rangle}\rangle$ and $|\tau_{|-i-i\rangle}\rangle$ both collapse into $\left(S\frac{I+iU}{2}\right)|\psi\rangle$ or $\left(S^\dagger\frac{I-iU}{2}\right)|\psi\rangle$ with equal probability. A formulation for the corresponding density matrix is shown in Equation (A.71).

$$\begin{aligned}\rho_{|ii\rangle} &= \left(S^\dagger \otimes \frac{I-iU}{2}\right)\rho\left(S^\dagger \otimes \frac{I-iU}{2}\right)^\dagger + \left(S \otimes \frac{I+iU}{2}\right)\rho\left(S \otimes \frac{I+iU}{2}\right)^\dagger \\ &= \rho_{|-i-i\rangle}\end{aligned} \tag{A.71}$$

From the calculations above, we can conclude that $\rho_{|++\rangle} = \rho_{|--\rangle}$ and $\rho_{|ii\rangle} = \rho_{|-i-i\rangle}$.

Finally, we prove Equation (3.19). The density matrices $\rho_{|++\rangle}$ and $\rho_{|ii\rangle}$ are shown in Equations (A.72) and (A.73) and their difference equating to E_ρ is shown in Equation (A.74).

$$\rho_{|++\rangle} = \frac{1}{2}\begin{bmatrix} au_0\overline{au_0} + au_0\overline{bu_1} + a\overline{a} + bu_1\overline{au_0} + bu_1\overline{bu_1} & au_0\overline{au_2} + au_0\overline{bu_3} + a\overline{b} + bu_1\overline{au_2} + bu_1\overline{bu_3} \\ au_2\overline{au_0} + au_2\overline{bu_1} + bu_3\overline{au_0} + bu_3\overline{bu_1} + b\overline{a} & au_2\overline{au_2} + au_2\overline{bu_3} + bu_3\overline{au_2} + bu_3\overline{bu_3} + b\overline{b} \\ cu_0\overline{a} + c\overline{au_0} + c\overline{bu_1} + du_1\overline{a} & cu_0\overline{b} + c\overline{au_2} + c\overline{bu_3} + du_1\overline{b} \\ cu_2\overline{a} + du_3\overline{a} + d\overline{au_0} + d\overline{bu_1} & cu_2\overline{b} + du_3\overline{b} + d\overline{au_2} + d\overline{bu_3} \end{bmatrix}$$
$$\begin{bmatrix} au_0\overline{c} + a\overline{cu_0} + a\overline{du_1} + bu_1\overline{c} & au_0\overline{d} + a\overline{cu_2} + a\overline{du_3} + bu_1\overline{d} \\ au_2\overline{c} + bu_3\overline{c} + b\overline{cu_0} + b\overline{du_1} & au_2\overline{d} + bu_3\overline{d} + b\overline{cu_2} + b\overline{du_3} \\ cu_0\overline{cu_0} + cu_0\overline{du_1} + c\overline{c} + du_1\overline{cu_0} + du_1\overline{du_1} & cu_0\overline{cu_2} + cu_0\overline{du_3} + c\overline{d} + du_1\overline{cu_2} + du_1\overline{du_3} \\ cu_2\overline{cu_0} + cu_2\overline{du_1} + du_3\overline{cu_0} + du_3\overline{du_1} + d\overline{c} & cu_2\overline{cu_2} + cu_2\overline{du_3} + du_3\overline{cu_2} + du_3\overline{du_3} + d\overline{d} \end{bmatrix} \tag{A.72}$$

$$\rho_{|ii\rangle} = \frac{1}{2}\begin{bmatrix} au_0\overline{au_0} + au_0\overline{bu_1} + a\overline{a} + bu_1\overline{au_0} + bu_1\overline{bu_1} & au_0\overline{au_2} + au_0\overline{bu_3} + a\overline{b} + bu_1\overline{au_2} + bu_1\overline{bu_3} \\ au_2\overline{au_0} + au_2\overline{bu_1} + bu_3\overline{au_0} + bu_3\overline{bu_1} + b\overline{a} & au_2\overline{au_2} + au_2\overline{bu_3} + bu_3\overline{au_2} + bu_3\overline{bu_3} + b\overline{b} \\ -cu_0\overline{a} + c\overline{au_0} + c\overline{bu_1} - du_1\overline{a} & -cu_0\overline{b} + c\overline{au_2} + c\overline{bu_3} - du_1\overline{b} \\ -cu_2\overline{a} - du_3\overline{a} + d\overline{au_0} + d\overline{bu_1} & -cu_2\overline{b} - du_3\overline{b} + d\overline{au_2} + d\overline{bu_3} \end{bmatrix}$$
$$\begin{bmatrix} au_0\overline{c} - a\overline{cu_0} - a\overline{du_1} + bu_1\overline{c} & au_0\overline{d} - a\overline{cu_2} - a\overline{du_3} + bu_1\overline{d} \\ au_2\overline{c} + bu_3\overline{c} - b\overline{cu_0} - b\overline{du_1} & au_2\overline{d} + bu_3\overline{d} - b\overline{cu_2} - b\overline{du_3} \\ cu_0\overline{cu_0} + cu_0\overline{du_1} + c\overline{c} + du_1\overline{cu_0} + du_1\overline{du_1} & cu_0\overline{cu_2} + cu_0\overline{du_3} + c\overline{d} + du_1\overline{cu_2} + du_1\overline{du_3} \\ cu_2\overline{cu_0} + cu_2\overline{du_1} + du_3\overline{cu_0} + du_3\overline{du_1} + d\overline{c} & cu_2\overline{cu_2} + cu_2\overline{du_3} + du_3\overline{cu_2} + du_3\overline{du_3} + d\overline{d} \end{bmatrix} \tag{A.73}$$

$$\rho_{|++\rangle} - \rho_{|ii\rangle} = \begin{bmatrix} 0 & 0 & a\left(\overline{cu_0} + \overline{du_1}\right) & a\left(\overline{cu_2} + \overline{du_3}\right) \\ 0 & 0 & b\left(\overline{cu_0} + \overline{du_1}\right) & b\left(\overline{cu_2} + \overline{du_3}\right) \\ (cu_0 + du_1)\,\overline{a} & (cu_0 + du_1)\,\overline{b} & 0 & 0 \\ (cu_2 + du_3)\,\overline{a} & (cu_2 + du_3)\,\overline{b} & 0 & 0 \end{bmatrix} = E_\rho \tag{A.74}$$

A.4 Circuit Simplification Condition

In this section, we calculate the difference between ρ'_G and $\rho_{(G\otimes G)|{+}{+}\rangle}$, which we need to derive the condition (Equation (3.32)) under which the equivalence depicted in Figure 3.4 is true. G is defined in Equation (3.23). As a first step, we calculate the pure states before measurements of each circuit applied to an arbitrary state $|\psi\rangle$ in Equations (A.75) to (A.87).

$$|\tau_{(G\otimes G)|{+}{+}\rangle}\rangle = CZ_{1,2}H_1CU_{1,3}CX_{0,1}CX_{2,0}G_1G_0\,(|{+}{+}\rangle\,|\psi\rangle) \tag{A.75}$$

$$= CZ_{1,2}H_1CU_{1,3}CX_{0,1}CX_{2,0}\left(\frac{1}{2}\left(\bigotimes_2(g\,|0\rangle + e^{i\varphi}\overline{g}\,|1\rangle)\right)\otimes|\psi\rangle\right) \tag{A.76}$$

$$\begin{aligned}= CZ_{1,2}H_1CU_{1,3}CX_{0,1}\Bigg(\frac{1}{2}\Bigg(&\left(\bigotimes_2(g\,|0\rangle + e^{i\varphi}\overline{g}\,|1\rangle)\right)\otimes(a\,|00\rangle + b\,|01\rangle)\\ &+ (e^{i\varphi}\overline{g}\,|0\rangle + g\,|1\rangle)\otimes(g\,|0\rangle + e^{i\varphi}\overline{g}\,|1\rangle)\otimes(c\,|10\rangle + d\,|11\rangle)\Bigg)\Bigg)\end{aligned} \tag{A.77}$$

$$\begin{aligned}= CZ_{1,2}H_1CU_{1,3}\Bigg(\frac{1}{2}(&((g\,|0\rangle\otimes(g\,|0\rangle + e^{i\varphi}\overline{g}\,|1\rangle)\\ &+ e^{i\varphi}\overline{g}\,|1\rangle\otimes(e^{i\varphi}\overline{g}\,|0\rangle + g\,|1\rangle))\otimes(a\,|00\rangle + b\,|01\rangle))\\ &+ (((e^{i\varphi}\overline{g}\,|0\rangle\otimes(g\,|0\rangle + e^{i\varphi}\overline{g}\,|1\rangle))\\ &+ (g\,|1\rangle\otimes(e^{i\varphi}\overline{g}\,|0\rangle + g\,|1\rangle))\otimes(c\,|10\rangle + d\,|11\rangle))\Bigg)\end{aligned} \tag{A.78}$$

$$\begin{aligned}= CZ_{1,2}H_1\Bigg(\frac{1}{2}(&(g^2\,|00\rangle + (e^{i\varphi}\overline{g})^2\,|10\rangle)\otimes(a\,|00\rangle + b\,|01\rangle)\\ &+ (ge^{i\varphi}\overline{g}\,|01\rangle + e^{i\varphi}\overline{g}g\,|11\rangle)\otimes((I\otimes U)(a\,|00\rangle + b\,|01\rangle))\\ &+ (e^{i\varphi}\overline{g}g\,|00\rangle + ge^{i\varphi}\overline{g}\,|10\rangle)\otimes(c\,|10\rangle + d\,|11\rangle)\\ &+ ((e^{i\varphi}\overline{g})^2\,|01\rangle + g^2\,|11\rangle)\otimes((I\otimes U)(c\,|10\rangle + d\,|11\rangle))\Bigg)\end{aligned} \tag{A.79}$$

$$\begin{aligned}= CZ_{1,2}\Bigg(\frac{1}{2}(&(g^2\,|0{+}\rangle + (e^{i\varphi}\overline{g})^2\,|1{+}\rangle)\otimes(a\,|00\rangle + b\,|01\rangle)\\ &+ (ge^{i\varphi}\overline{g}\,|0{-}\rangle + e^{i\varphi}\overline{g}g\,|1{-}\rangle)\otimes((I\otimes U)(a\,|00\rangle + b\,|01\rangle))\\ &+ (e^{i\varphi}\overline{g}g\,|0{+}\rangle + ge^{i\varphi}\overline{g}\,|1{+}\rangle)\otimes(c\,|10\rangle + d\,|11\rangle)\\ &+ ((e^{i\varphi}\overline{g})^2\,|0{-}\rangle + g^2\,|1{-}\rangle)\otimes((I\otimes U)(c\,|10\rangle + d\,|11\rangle))\Bigg)\end{aligned} \tag{A.80}$$

$$\begin{aligned}= \frac{1}{2}(&(g^2\,|0{+}\rangle + (e^{i\varphi}\overline{g})^2\,|1{+}\rangle)\otimes(a\,|00\rangle + b\,|01\rangle)\\ &+ (ge^{i\varphi}\overline{g}(|0{-}\rangle + |1{-}\rangle))\otimes((I\otimes U)(a\,|00\rangle + b\,|01\rangle))\\ &+ (e^{i\varphi}\overline{g}g(|0{-}\rangle + |1{-}\rangle))\otimes(c\,|10\rangle + d\,|11\rangle)\\ &+ ((e^{i\varphi}\overline{g})^2\,|0{+}\rangle + g^2\,|1{+}\rangle)\otimes((I\otimes U)(c\,|10\rangle + d\,|11\rangle))\end{aligned} \tag{A.81}$$

$$|\tau'_G\rangle = G_1 CZ_{0,1} H_0 CU_{0,2} G_0 \left(|+\rangle |\psi\rangle\right) \tag{A.82}$$

$$= G_1 CZ_{0,1} H_0 CU_{0,2} \left(\frac{1}{\sqrt{2}}((g|0\rangle + e^{i\varphi}\overline{g}|1\rangle) \otimes |\psi\rangle)\right) \tag{A.83}$$

$$= G_1 CZ_{0,1} H_0 \left(\frac{1}{\sqrt{2}}(g|0\rangle \otimes |\psi\rangle + e^{i\varphi}\overline{g}|1\rangle \otimes ((I\otimes U)|\psi\rangle))\right) \tag{A.84}$$

$$= G_1 CZ_{0,1} \left(\frac{1}{\sqrt{2}}(g|+\rangle \otimes |\psi\rangle + (e^{i\varphi}\overline{g}|-\rangle \otimes ((I\otimes U)|\psi\rangle)))\right) \tag{A.85}$$

$$\begin{aligned} = G_1 \Bigg(&\frac{1}{2}(g|0\rangle \otimes |\psi\rangle + (e^{i\varphi}\overline{g}|0\rangle \otimes ((I\otimes U)|\psi\rangle)) \\ &+ g|1\rangle \otimes ((Z\otimes I)|\psi\rangle) - (e^{i\varphi}\overline{g}|1\rangle \otimes ((Z\otimes U)|\psi\rangle))\Bigg) \end{aligned} \tag{A.86}$$

$$\begin{aligned} = &\frac{1}{\sqrt{2}}(g|+\rangle \otimes g(a|00\rangle + b|01\rangle) + e^{i\varphi}\overline{g}|-\rangle \otimes ((I\otimes U)g(a|00\rangle + b|01\rangle)) \\ &+ g|-\rangle \otimes e^{i\varphi}\overline{g}(c|10\rangle + d|11\rangle) + e^{i\varphi}\overline{g}|+\rangle \otimes ((I\otimes U)e^{i\varphi}\overline{g}(c|10\rangle + d|11\rangle))) \end{aligned} \tag{A.87}$$

Since the density matrices take up a lot of space to write down, we depict them as block matrices in Equations (A.88) to (A.97).

$$\rho_{(G\otimes G)|++\rangle} = \frac{1}{2}\begin{bmatrix} T_0 & T_1 \\ T_2 & T_3 \end{bmatrix} \tag{A.88}$$

$$T_0 = \begin{bmatrix} g^2\left(au_0\overline{au_0} + au_0\overline{b}\overline{u_1} + a\overline{a} + bu_1\overline{au_0} + bu_1\overline{b}\overline{u_1}\right)\overline{g}^2 & \\ g^2\left(au_2\overline{au_0} + au_2\overline{b}\overline{u_1} + bu_3\overline{au_0} + bu_3\overline{b}\overline{u_1} + b\overline{a}\right)\overline{g}^2 & \\ & g^2\left(au_0\overline{au_2} + au_0\overline{b}\overline{u_3} + a\overline{b} + bu_1\overline{au_2} + bu_1\overline{b}\overline{u_3}\right)\overline{g}^2 \\ & g^2\left(au_2\overline{au_2} + au_2\overline{b}\overline{u_3} + bu_3\overline{au_2} + bu_3\overline{b}\overline{u_3} + b\overline{b}\right)\overline{g}^2 \end{bmatrix} \tag{A.89}$$

$$T_1 = \frac{1}{2}\begin{bmatrix} \left(ag^4\overline{cu_0} + ag^4\overline{d}\overline{u_1} + \left(2ag^2u_0\overline{c} + ae^{2i\varphi}\overline{cg}^2\overline{u_0} + ae^{2i\varphi}\overline{d}\overline{g}^2\overline{u_1} + 2bg^2u_1\overline{c}\right)e^{2i\varphi}\overline{g}^2\right)e^{-2i\varphi} & \\ \left(bg^4\overline{cu_0} + bg^4\overline{d}\overline{u_1} + \left(2ag^2u_2\overline{c} + 2bg^2u_3\overline{c} + be^{2i\varphi}\overline{cg}^2\overline{u_0} + be^{2i\varphi}\overline{d}\overline{g}^2\overline{u_1}\right)e^{2i\varphi}\overline{g}^2\right)e^{-2i\varphi} & \\ & \left(ag^4\overline{cu_2} + ag^4\overline{d}\overline{u_3} + \left(2ag^2u_0\overline{d} + ae^{2i\varphi}\overline{cg}^2\overline{u_2} + ae^{2i\varphi}\overline{d}\overline{g}^2\overline{u_3} + 2bg^2u_1\overline{d}\right)e^{2i\varphi}\overline{g}^2\right)e^{-2i\varphi} \\ & \left(bg^4\overline{cu_2} + bg^4\overline{d}\overline{u_3} + \left(2ag^2u_2\overline{d} + 2bg^2u_3\overline{d} + be^{2i\varphi}\overline{cg}^2\overline{u_2} + be^{2i\varphi}\overline{d}\overline{g}^2\overline{u_3}\right)e^{2i\varphi}\overline{g}^2\right)e^{-2i\varphi} \end{bmatrix} \tag{A.90}$$

$$T_2 = \frac{1}{2}\begin{bmatrix} \left(cg^4u_0\overline{a} + dg^4u_1\overline{a} + \left(2cg^2\overline{au_0} + 2cg^2\overline{b}\overline{u_1} + cu_0e^{2i\varphi}\overline{ag}^2 + du_1e^{2i\varphi}\overline{ag}^2\right)e^{2i\varphi}\overline{g}^2\right)e^{-2i\varphi} & \\ \left(cg^4u_2\overline{a} + dg^4u_3\overline{a} + \left(cu_2e^{2i\varphi}\overline{ag}^2 + 2dg^2\overline{au_0} + 2dg^2\overline{b}\overline{u_1} + du_3e^{2i\varphi}\overline{ag}^2\right)e^{2i\varphi}\overline{g}^2\right)e^{-2i\varphi} & \\ & \left(cg^4u_0\overline{b} + dg^4u_1\overline{b} + \left(2cg^2\overline{au_2} + 2cg^2\overline{b}\overline{u_3} + cu_0e^{2i\varphi}\overline{b}\overline{g}^2 + du_1e^{2i\varphi}\overline{b}\overline{g}^2\right)e^{2i\varphi}\overline{g}^2\right)e^{-2i\varphi} \\ & \left(cg^4u_2\overline{b} + dg^4u_3\overline{b} + \left(cu_2e^{2i\varphi}\overline{b}\overline{g}^2 + 2dg^2\overline{au_2} + 2dg^2\overline{b}\overline{u_3} + du_3e^{2i\varphi}\overline{b}\overline{g}^2\right)e^{2i\varphi}\overline{g}^2\right)e^{-2i\varphi} \end{bmatrix} \tag{A.91}$$

$$T_3 = \begin{bmatrix} g^2\left(cu_0\overline{cu_0} + cu_0\overline{du_1} + c\overline{c} + du_1\overline{cu_0} + du_1\overline{du_1}\right)\overline{g}^2 \\ g^2\left(cu_2\overline{cu_0} + cu_2\overline{du_1} + du_3\overline{cu_0} + du_3\overline{du_1} + d\overline{c}\right)\overline{g}^2 \end{bmatrix} \\ \begin{bmatrix} g^2\left(cu_0\overline{cu_2} + cu_0\overline{du_3} + c\overline{d} + du_1\overline{cu_2} + du_1\overline{du_3}\right)\overline{g}^2 \\ g^2\left(cu_2\overline{cu_2} + cu_2\overline{du_3} + du_3\overline{cu_2} + du_3\overline{du_3} + d\overline{d}\right)\overline{g}^2 \end{bmatrix} \tag{A.92}$$

$$\rho'_G = \frac{1}{2}\begin{bmatrix} T'_0 & T'_1 \\ T'_2 & T'_3 \end{bmatrix} \tag{A.93}$$

$$T'_0 = \begin{bmatrix} g^2\left(au_0\overline{au_0} + au_0\overline{bu_1} + a\overline{a} + bu_1\overline{au_0} + bu_1\overline{bu_1}\right)\overline{g}^2 \\ g^2\left(au_2\overline{au_0} + au_2\overline{bu_1} + bu_3\overline{au_0} + bu_3\overline{bu_1} + b\overline{a}\right)\overline{g}^2 \end{bmatrix} \\ \begin{bmatrix} g^2\left(au_0\overline{au_2} + au_0\overline{bu_3} + a\overline{b} + bu_1\overline{au_2} + bu_1\overline{bu_3}\right)\overline{g}^2 \\ g^2\left(au_2\overline{au_2} + au_2\overline{bu_3} + bu_3\overline{au_2} + bu_3\overline{bu_3} + b\overline{b}\right)\overline{g}^2 \end{bmatrix} \tag{A.94}$$

$$T'_1 = \begin{bmatrix} g^2\left(ag^2\overline{cu_0} + ag^2\overline{du_1} + au_0e^{2i\varphi}\overline{cg}^2 + bu_1e^{2i\varphi}\overline{cg}^2\right)e^{-2i\varphi} \\ g^2\left(au_2e^{2i\varphi}\overline{cg}^2 + bg^2\overline{cu_0} + bg^2\overline{du_1} + bu_3e^{2i\varphi}\overline{cg}^2\right)e^{-2i\varphi} \end{bmatrix} \\ \begin{bmatrix} g^2\left(ag^2\overline{cu_2} + ag^2\overline{du_3} + au_0e^{2i\varphi}\overline{dg}^2 + bu_1e^{2i\varphi}\overline{dg}^2\right)e^{-2i\varphi} \\ g^2\left(au_2e^{2i\varphi}\overline{dg}^2 + bg^2\overline{cu_2} + bg^2\overline{du_3} + bu_3e^{2i\varphi}\overline{dg}^2\right)e^{-2i\varphi} \end{bmatrix} \tag{A.95}$$

$$T'_2 = \begin{bmatrix} \left(cg^2\overline{au_0} + cg^2\overline{bu_1} + cu_0e^{2i\varphi}\overline{ag}^2 + du_1e^{2i\varphi}\overline{ag}^2\right)\overline{g}^2 \\ \left(cu_2e^{2i\varphi}\overline{ag}^2 + dg^2\overline{au_0} + dg^2\overline{bu_1} + du_3e^{2i\varphi}\overline{ag}^2\right)\overline{g}^2 \end{bmatrix} \\ \begin{bmatrix} \left(cg^2\overline{au_2} + cg^2\overline{bu_3} + cu_0e^{2i\varphi}\overline{bg}^2 + du_1e^{2i\varphi}\overline{bg}^2\right)\overline{g}^2 \\ \left(cu_2e^{2i\varphi}\overline{bg}^2 + dg^2\overline{au_2} + dg^2\overline{bu_3} + du_3e^{2i\varphi}\overline{bg}^2\right)\overline{g}^2 \end{bmatrix} \tag{A.96}$$

$$T'_3 = \begin{bmatrix} g^2\left(au_0\overline{au_0} + au_0\overline{bu_1} + a\overline{a} + bu_1\overline{au_0} + bu_1\overline{bu_1}\right)\overline{g}^2 \\ g^2\left(au_2\overline{au_0} + au_2\overline{bu_1} + bu_3\overline{au_0} + bu_3\overline{bu_1} + b\overline{a}\right)\overline{g}^2 \end{bmatrix} \\ \begin{bmatrix} g^2\left(au_0\overline{au_2} + au_0\overline{bu_3} + a\overline{b} + bu_1\overline{au_2} + bu_1\overline{bu_3}\right)\overline{g}^2 \\ g^2\left(au_2\overline{au_2} + au_2\overline{bu_3} + bu_3\overline{au_2} + bu_3\overline{bu_3} + b\overline{b}\right)\overline{g}^2 \end{bmatrix} \tag{A.97}$$

The difference between ρ'_G and $\rho_{(G\otimes G)|{+}{+}\rangle}$ is shown in Equations (A.98) and (A.99).

$$\rho'_G - \rho_{(G\otimes G)|{+}{+}\rangle} = \begin{bmatrix} T'_0 - T_0 & T'_1 - T_1 \\ T'_2 - T_2 & T'_3 - T_3 \end{bmatrix} \tag{A.98}$$

$$= \frac{1}{4}\left(g^4 - e^{4i\varphi}\overline{g}^4\right)e^{-2i\varphi}\begin{bmatrix} 0 & E_T \\ -E_T^\dagger & 0 \end{bmatrix} \tag{A.99}$$

E_T is defined in Equation (A.100).

$$E_T = \begin{bmatrix} a\left(\overline{cu_0} + \overline{d}\overline{u_1}\right) & a\left(\overline{cu_2} + \overline{d}\overline{u_3}\right) \\ b\left(\overline{cu_0} + \overline{d}\overline{u_1}\right) & b\left(\overline{cu_2} + \overline{d}\overline{u_3}\right) \end{bmatrix} \tag{A.100}$$

The condition under which we can eliminate Alice's ancilla qubit in the compensation circuits is derived in Section 3.2.

A.5 Compensation Circuit Decomposition for Controlled-$\{X, Y, Z, H\}$

To proof the decompositions from Figures 3.9a and 3.9b, we substitute the $u_{i\in\{0,1,2,3\}}$ from U in $\rho_{|{+}{+}\rangle}$ (Equation (A.72)) and $\rho_{|ii\rangle}$ (Equation (A.73)) by the corresponding entries of the X, Y, Z, and H matrices. This results in the density matrix of the corresponding compensation circuit applied to an arbitrary state $|\psi\rangle$ as defined in Equation (3.2). Then we sum up the $s_i^G, i \in \{0, \ldots, 9\}, G \in \{X, Y, Z, H\}(\rho)$ (Equation (A.2)) density matrices according to the respective decomposition and verify that they are equal to the substituted corresponding $\rho_{|\cdot,\cdot\rangle}$ density matrix. Equations (A.101) to (A.108) comprise the equivalence of the $C(|{+}\rangle)$ decomposition (Figure 3.9a) for the four gates X, Y, Z, and H.

$$\rho_{|{+}{+}\rangle} \overset{U=X}{=} \frac{1}{2}\begin{bmatrix} a\overline{a} + b\overline{b} & a\overline{b} + b\overline{a} & a\overline{d} + b\overline{c} & a\overline{c} + b\overline{d} \\ a\overline{b} + b\overline{a} & a\overline{a} + b\overline{b} & a\overline{c} + b\overline{d} & a\overline{d} + b\overline{c} \\ c\overline{b} + d\overline{a} & c\overline{a} + d\overline{b} & c\overline{c} + d\overline{d} & c\overline{d} + d\overline{c} \\ c\overline{a} + d\overline{b} & c\overline{b} + d\overline{a} & c\overline{d} + d\overline{c} & c\overline{c} + d\overline{d} \end{bmatrix} \tag{A.101}$$

$$= \frac{1}{2}\left(\sum_{i\in 2,4,5,6,7,8} s_i^X(\rho) - \sum_{i\in\{3,9\}} s_i^X(\rho)\right) \tag{A.102}$$

$$\rho_{|{+}{+}\rangle} \overset{U=Y}{=} \frac{1}{2}\begin{bmatrix} a\overline{a} + b\overline{b} & a\overline{b} - b\overline{a} & i\left(a\overline{d} - b\overline{c}\right) & i\left(-a\overline{c} - b\overline{d}\right) \\ -a\overline{b} + b\overline{a} & a\overline{a} + b\overline{b} & i\left(a\overline{c} + b\overline{d}\right) & i\left(a\overline{d} - b\overline{c}\right) \\ i\left(c\overline{b} - d\overline{a}\right) & i\left(-c\overline{a} - d\overline{b}\right) & c\overline{c} + d\overline{d} & c\overline{d} - d\overline{c} \\ i\left(c\overline{a} + d\overline{b}\right) & i\left(c\overline{b} - d\overline{a}\right) & -c\overline{d} + d\overline{c} & c\overline{c} + d\overline{d} \end{bmatrix} \tag{A.103}$$

$$= \frac{1}{2}\left(\sum_{i\in 2,4,5,6,7,8} s_i^Y(\rho) - \sum_{i\in\{3,9\}} s_i^Y(\rho)\right) \tag{A.104}$$

$$\rho_{|{+}{+}\rangle} \overset{U=Z}{=} \begin{bmatrix} a\overline{a} & 0 & a\overline{c} & 0 \\ 0 & b\overline{b} & 0 & -b\overline{d} \\ c\overline{a} & 0 & c\overline{c} & 0 \\ 0 & -d\overline{b} & 0 & d\overline{d} \end{bmatrix} \tag{A.105}$$

$$= \frac{1}{2}\left(\sum_{i\in 2,4,5,6,7,8} s_i^Z(\rho) - \sum_{i\in\{3,9\}} s_i^Z(\rho) \right) \tag{A.106}$$

$$\rho_{|{+}{+}\rangle} \overset{U=H}{=} \frac{1}{4} \begin{bmatrix} 3a\overline{a} + a\overline{b} + b\overline{a} + b\overline{b} & a\overline{a} + a\overline{b} + b\overline{a} - b\overline{b} \\ a\overline{a} + a\overline{b} + b\overline{a} - b\overline{b} & a\overline{a} - a\overline{b} - b\overline{a} + 3b\overline{b} \\ \sqrt{2}\cdot\left(2c\overline{a} + c\overline{b} + d\overline{a}\right) & \sqrt{2}\left(c\overline{a} + d\overline{b}\right) \\ \sqrt{2}\left(c\overline{a} + d\overline{b}\right) & \sqrt{2}\left(c\overline{b} + d\overline{a} - 2d\overline{b}\right) \end{bmatrix}$$
$$\begin{bmatrix} \sqrt{2}\cdot\left(2a\overline{c} + a\overline{d} + b\overline{c}\right) & \sqrt{2}\left(a\overline{c} + b\overline{d}\right) \\ \sqrt{2}\left(a\overline{c} + b\overline{d}\right) & \sqrt{2}\left(a\overline{d} + b\overline{c} - 2b\overline{d}\right) \\ 3c\overline{c} + c\overline{d} + d\overline{c} + d\overline{d} & c\overline{c} + c\overline{d} + d\overline{c} - d\overline{d} \\ c\overline{c} + c\overline{d} + d\overline{c} - d\overline{d} & c\overline{c} - c\overline{d} - d\overline{c} + 3d\overline{d} \end{bmatrix} \tag{A.107}$$

$$= \frac{1}{2}\left(\sum_{i\in 2,4,5,6,7,8} s_i^H(\rho) - \sum_{i\in\{3,9\}} s_i^H(\rho) \right) \tag{A.108}$$

Equations (A.109) to (A.116) comprise the equivalence of the $C(|i\rangle)$ decomposition (Figure 3.9b) for the four gates X, Y, Z, and H.

$$\rho_{|ii\rangle} \overset{U=X}{=} \frac{1}{2} \begin{bmatrix} a\overline{a} + b\overline{b} & a\overline{b} + b\overline{a} & -a\overline{d} + b\overline{c} & -a\overline{c} + b\overline{d} \\ a\overline{b} + b\overline{a} & a\overline{a} + b\overline{b} & a\overline{c} - b\overline{d} & a\overline{d} - b\overline{c} \\ c\overline{b} - d\overline{a} & c\overline{a} - d\overline{b} & c\overline{c} + d\overline{d} & c\overline{d} + d\overline{c} \\ -c\overline{a} + d\overline{b} & -c\overline{b} + d\overline{a} & c\overline{d} + d\overline{c} & c\overline{c} + d\overline{d} \end{bmatrix} \tag{A.109}$$

$$= \frac{1}{2}\left(\sum_{i=2}^{9} s_i^X(\rho) - \sum_{i\in\{0,1\}} s_i^X(\rho) \right) \tag{A.110}$$

$$\rho_{|ii\rangle} \overset{U=Y}{=} \frac{1}{2} \begin{bmatrix} a\overline{a} + b\overline{b} & a\overline{b} - b\overline{a} & i\left(-a\overline{d} - b\overline{c}\right) & i\left(a\overline{c} - b\overline{d}\right) \\ -a\overline{b} + b\overline{a} & a\overline{a} + b\overline{b} & i\left(a\overline{c} - b\overline{d}\right) & i\left(a\overline{d} + b\overline{c}\right) \\ i\left(c\overline{b} + d\overline{a}\right) & i\left(-c\overline{a} + d\overline{b}\right) & c\overline{c} + d\overline{d} & c\overline{d} - d\overline{c} \\ i\left(-c\overline{a} + d\overline{b}\right) & i\left(-c\overline{b} - d\overline{a}\right) & -c\overline{d} + d\overline{c} & c\overline{c} + d\overline{d} \end{bmatrix} \tag{A.111}$$

$$= \frac{1}{2}\left(\sum_{i=2}^{9} s_i^Y(\rho) - \sum_{i\in\{0,1\}} s_i^Y(\rho) \right) \tag{A.112}$$

$$\rho_{|ii\rangle} \overset{U=Z}{=} \begin{bmatrix} a\overline{a} & 0 & 0 & a\overline{d} \\ 0 & b\overline{b} & -b\overline{c} & 0 \\ 0 & -c\overline{b} & c\overline{c} & 0 \\ d\overline{a} & 0 & 0 & d\overline{d} \end{bmatrix} \tag{A.113}$$

$$= \frac{1}{2}\left(\sum_{i=2}^{9} s_i^Z(\rho) - \sum_{i\in\{0,1\}} s_i^Z(\rho)\right) \tag{A.114}$$

$$\rho_{|ii\rangle} \overset{U=H}{=} \frac{1}{4}\begin{bmatrix} 3a\overline{a} + a\overline{b} + b\overline{a} + b\overline{b} & a\overline{a} + a\overline{b} + b\overline{a} - b\overline{b} \\ a\overline{a} + a\overline{b} + b\overline{a} - b\overline{b} & a\overline{a} - a\overline{b} - b\overline{a} + 3b\overline{b} \\ \sqrt{2}\left(c\overline{b} - d\overline{a}\right) & \sqrt{2}\left(c\overline{a} - 2c\overline{b} - d\overline{b}\right) \\ \sqrt{2}\left(-c\overline{a} + 2d\overline{a} + d\overline{b}\right) & \sqrt{2}\left(-c\overline{b} + d\overline{a}\right) \end{bmatrix}$$
$$\begin{bmatrix} \sqrt{2}\left(-a\overline{d} + b\overline{c}\right) & \sqrt{2}\left(-a\overline{c} + 2a\overline{d} + b\overline{d}\right) \\ \sqrt{2}\left(a\overline{c} - 2b\overline{c} - b\overline{d}\right) & \sqrt{2}\left(a\overline{d} - b\overline{c}\right) \\ 3c\overline{c} + c\overline{d} + d\overline{c} + d\overline{d} & c\overline{c} + c\overline{d} + d\overline{c} - d\overline{d} \\ c\overline{c} + c\overline{d} + d\overline{c} - d\overline{d} & c\overline{c} - c\overline{d} - d\overline{c} + 3d\overline{d} \end{bmatrix} \tag{A.115}$$

$$= \frac{1}{2}\left(\sum_{i=2}^{9} s_i^H(\rho) - \sum_{i\in\{0,1\}} s_i^H(\rho)\right) \tag{A.116}$$

The verification for the decomposition from Figure 3.9c works analogously. We substitute the X, Y, Z, and H gates into the difference of $\rho_{|++\rangle}$ and $\rho_{|ii\rangle}$ (Equation (3.19)) and check if it is the same as the combination of the corresponding density matrices. We do so in Equations (A.117) to (A.124).

$$E_\rho \overset{U=X}{=} \begin{bmatrix} 0 & 0 & a\overline{d} & a\overline{c} \\ 0 & 0 & b\overline{d} & b\overline{c} \\ d\overline{a} & d\overline{b} & 0 & 0 \\ c\overline{a} & c\overline{b} & 0 & 0 \end{bmatrix} \tag{A.117}$$

$$= \frac{1}{2}\left(s_0^X(\rho) + s_1^X(\rho)\right) - s_3^X(\rho) - s_9^X(\rho) \tag{A.118}$$

$$E_\rho \overset{U=Y}{=} \begin{bmatrix} 0 & 0 & ia\overline{d} & -ia\overline{c} \\ 0 & 0 & ib\overline{d} & -ib\overline{c} \\ -id\overline{a} & -id\overline{b} & 0 & 0 \\ ic\overline{a} & ic\overline{b} & 0 & 0 \end{bmatrix} \tag{A.119}$$

$$= \frac{1}{2}\left(s_0^Y(\rho) + s_1^Y(\rho)\right) - s_3^Y(\rho) - s_9^Y(\rho) \tag{A.120}$$

$$E_\rho \overset{U=Z}{=} \begin{bmatrix} 0 & 0 & a\overline{c} & -a\overline{d} \\ 0 & 0 & b\overline{c} & -b\overline{d} \\ c\overline{a} & c\overline{b} & 0 & 0 \\ -d\overline{a} & -d\overline{b} & 0 & 0 \end{bmatrix} \tag{A.121}$$

$$= \frac{1}{2}\left(s_0^Z(\rho) + s_1^Z(\rho)\right) - s_3^Z(\rho) - s_9^Z(\rho) \tag{A.122}$$

$$E_\rho \overset{U=H}{=} \frac{1}{\sqrt{2}} \begin{bmatrix} 0 & 0 & a\left(\overline{c}+\overline{d}\right) & a\left(\overline{c}-\overline{d}\right) \\ 0 & 0 & b\left(\overline{c}+\overline{d}\right) & b\left(\overline{c}-\overline{d}\right) \\ (c+d)\,\overline{a} & (c+d)\,\overline{b} & 0 & 0 \\ (c-d)\,\overline{a} & (c-d)\,\overline{b} & 0 & 0 \end{bmatrix} \tag{A.123}$$

$$= \frac{1}{2}\left(s_0^H(\rho) + s_1^H(\rho)\right) - s_3^H(\rho) - s_9^H(\rho) \tag{A.124}$$

Declaration

I hereby declare that the work presented in this thesis is entirely my own and that I did not use any other sources and references than the listed ones. I have marked all direct or indirect statements from other sources contained therein as quotations. Neither this work nor significant parts of it were part of another examination procedure. I have not published this work in whole or in part before. The electronic copy is consistent with all submitted copies.

---

place, date, signature